

Cavitation control using passive flow control techniques

Cite as: Phys. Fluids **33**, 121301 (2021); <https://doi.org/10.1063/5.0071781>

Submitted: 16 September 2021 • Accepted: 12 November 2021 • Published Online: 16 December 2021

 Mahshid Zaresharif,  Florent Ravelet,  David J. Kinahan, et al.



View Online



Export Citation



CrossMark

ARTICLES YOU MAY BE INTERESTED IN

[Numerical validation of the dusty-gas model for binary diffusion in low aspect ratio capillaries](#)
Physics of Fluids **33**, 121701 (2021); <https://doi.org/10.1063/5.0072800>

[Experimentally probing the extremes of droplet-on-demand printability via liquid metals](#)
Physics of Fluids **33**, 121708 (2021); <https://doi.org/10.1063/5.0076594>

[Control of unsteady partial cavitation and cloud cavitation in marine engineering and hydraulic systems](#)
Physics of Fluids **32**, 052108 (2020); <https://doi.org/10.1063/5.0006560>

Physics of Fluids

Submit Today!

Special Topic: Hydrogen Flame and Detonation Physics



Cavitation control using passive flow control techniques

Cite as: Phys. Fluids **33**, 121301 (2021); doi: [10.1063/5.0071781](https://doi.org/10.1063/5.0071781)

Submitted: 16 September 2021 · Accepted: 12 November 2021 ·

Published Online: 16 December 2021



View Online



Export Citation



CrossMark

Mahshid Zaresharif,^{1,2} Florent Ravelet,³ David J. Kinahan,^{1,2,4,5} and Yan M. C. Delaure^{1,2,a)}

AFFILIATIONS

¹Dublin City University, School of Mechanical and Manufacturing Engineering, DCU Water Institute, Dublin D09 V209 9, Ireland

²Dublin City University, School of Mechanical and Manufacturing Engineering, Advanced Processing Technology Research Centre, Dublin, D09 V209 9, Ireland

³Arts et Metiers Institute of Technology, CNAM, LIFSE, HESAM University, 75013 Paris, France

⁴I-Form-The SFI Centre for Advanced Manufacturing, Dublin City University, D09 V209 9, Ireland

⁵National Centre for Sensor Research, Dublin City University, D09 V209 9, Ireland

^{a)} Author to whom correspondence should be addressed: Yan.Delaure@dcu.ie

ABSTRACT

Passive flow control techniques, and particularly vortex generators have been used successfully in a broad range of aero- and hydrodynamics applications to alter the characteristics of boundary layer separation. This study aims to review how such techniques can mitigate the extent and impact of cavitation in incompressible flows. This review focuses first on vortex generators to characterize key physical principles. It then considers the complete range of passive flow control technologies, including surface conditioning and roughness, geometry modification, grooves, discharge, injection, obstacles, vortex generators, and bubble generators. The passive flow control techniques reviewed typically delay and suppress boundary layer separation by decreasing the pressure gradient at the separation point. The literature also identifies streamwise vortices that result in the transfer of momentum from the free stream to near-wall low energy flow regions. The area of interest concerns hydraulic machinery, whose performance and life span are particularly susceptible to cavitation. The impact on performance includes a reduction in efficiency and fluctuations in discharge pressure and flow, while cavitation can greatly increase wear of bearings, wearing rings, seals, and impeller surfaces due to excessive vibration and surface erosion. In that context, few studies have also shown the positive effects that passive controls can have on the hydraulic performance of centrifugal pumps, such as total head and efficiency. It is conceivable that a new generation of design in hydraulic systems may be possible if simple design features can be conceived to maximize power transfer and minimize losses and cavitation. There are still, however, significant research gaps in understanding a range of impact factors such as manufacturing processes, lifetime, and durability, and essentially how a static design can be optimized to deliver improved performance over a realistic range of operating conditions.

© 2021 Author(s). All article content, except where otherwise noted, is licensed under a Creative Commons Attribution (CC BY) license (<http://creativecommons.org/licenses/by/4.0/>). <https://doi.org/10.1063/5.0071781>

NOMENCLATURE

ACL	Anti-cavitation lip	l	Device chord length
c	Hydrofoil chord	L	Distance between two counter-rotating vortex generators' ends
CGs	Cavitating bubble generators	LSB	Laminar separation bubble
CCGs	Cylindrical cavitating bubble generators	m	Vortex generators spacing in the spanwise direction between two pair of counter-rotating vortex generators
C_{pmin}	Minimum pressure coefficient	mVG	Micro-vortex generator
GEMS	Gas entrapment by micro-textured surfaces	n	Gap ratio of between two counter-rotating vanes
h	Device height	NPSH	Net positive suction head
h/	δ Device height to boundary layer thickness ratio	OHG	Overhanging grooves
K-H	Kelvin-Helmholtz	PIV	Particle image velocimetry

Ra	Roughness
Re	Reynolds number
Re_θ	Reynolds number based on momentum thickness
R-T	Rayleigh–Taylor
S	Hydrofoil span
TLV	Tip-leakage vortex
U_∞	Free-stream streamwise velocity
VG	Vortex generator
X_{VG}	Distance between the leading edge and vortex generators
z	Distance between two doublet wheeler or wishbone wheeler vortex generators
α	Angle of attack
β	Device angle of incidence
δ	Boundary layer thickness
Δh	Height of the cavity
Δs	Distance between the leading edge roughness and the re-entrant jets
ΔX_{VG}	Distance between the vortex generators trailing edge and baseline separation line
λ	Distance between two co-rotating vortex generators
σ	Cavitation number

I. INTRODUCTION

Cavitation is defined as the appearance of vapor cavities due to the phase change in a liquid medium.¹ Hydraulic machinery in industries has been experiencing many challenges that are associated with the cavitation phenomenon, including noise,² vibration,³ material damage,⁴ and reduced efficiency/performance.⁵

Since the initial investigation of Reynolds,⁶ there have been many studies that have attempted to improve our understanding of the nature of the phenomenon; focusing, among others, on processes involved in the formation of cavitation vapor, the dynamics of bubble detachment, the behavior of boundary layers, and, more recently, on how the strength, extent, dynamics, and impact of cavitation may be controlled or mitigated. The two essential prerequisite conditions needed for cavitation to develop are the presence of favorable bubble inception sites and the opportunity for the liquid pressure to fall below the saturation pressure. Dissolved gas in the liquid medium can also play a role in the activation of nucleation sites. These prerequisites commonly occur in hydraulic machinery. Sudden pressure drops over impellers and blades occur as the energy in the flow is transferred to kinetic energy in the volute and around the impeller blades.⁷

Initially, the bubbles in the oncoming stream on a hydrofoil or generally a surface were assumed to be micrometer-sized nuclei in the liquid and they would move along the streamline close to the solid surface. Observable bubbles of 1 mm or larger were deemed to initiate cavitation. Nuclei present in incident-free streams are a primary source of these bubbles. Nuclei passing close to the front stagnation point will experience large fluid accelerations and pressure gradients since the streamlines encountering the low-pressure region are close to the surface. The initial growth phase in all cases was characterized by a spherical cap. Bubbles are separated from walls by thin layers of liquid of a thickness equal to the boundary layer. Once the bubble enters an area of adverse pressure gradient, it begins to be pushed inward, resulting in a wedge-shaped profile. Thus, the bubble collapse begins on the exterior frontal surface, often resulting in the bubble breaking into

forward and aft bubbles. This phase is called bubble traveling cavitation.^{8–10}

As the bubble grows, it develops substantial spanwise vorticity as it interacts with the boundary layer. As a result, the cavitating vorticity within a bubble is concentrated as the collapse proceeds, transforming it into one (or several, or even more) cavitating vortex with a spanwise axis. When the vortex bubbles collapse, they reappear as a cloud of small bubbles. There is an occasional occurrence where bubbles pass the point where the laminar separation occurs and subsequently develop locally attached cavitation streaks at the lateral or spanwise extremities of the bubble.

This trailing edge of attached cavitation, which is attached to the solid surface, eventually extends out behind the main bubble. Consequently, the main bubble collapses first, leaving the tails to persist for a fraction longer. At this point, an attached cavity is generated, which can evolve to other type of cavitation such as cloud cavitation or supercavitation (Table II).^{9,11}

Once formed, cavities will eventually collapse or release clouds that will collapse resulting in a shock wave¹² and focus of energy toward walls, which typically lead to cavitation erosion and noise. Over the past four decades, significant research effort has been dedicated to investigate how cavitation may be controlled. This work has tended to focus on extruded profiles from hydrofoils, propellers, pumps, and turbine blades.

Stabilizing cavity resonance or reducing volume of wall and near wall cavities are two solutions to control, reduce, or eliminate cavitation. The presence of nuclei and micro-bubbles within liquids and at solid surfaces, surface characteristics, and Reynolds number are some factors that affect cavitation.^{13–17} Adjustment or modification of one or all of these parameters can allow for effective cavitation control. However, the most important parameters which impact cavitation have been linked to the control of boundary layer separation.^{1,18,19}

The laminar separation can be generated downstream of an adverse pressure gradient and make a low pressure region. The separated layer can then shelter the oncoming flow and generate an attached separation cavity with low pressure at the core. It was found that suppressing or eliminating this separation can effectively delay or suppress the formation of an attached cavity.²⁰ The higher momentum of the turbulent flow improves its ability to resist adverse pressure gradient over convex surfaces and, hence, limit the incidence of separation.^{1,21} Compared to turbulent boundary conditions, a laminar boundary flow is more likely to separate, resulting in a higher drag penalty. The control of boundary layer separation achieved by triggering an early transition to a turbulent boundary layer is, therefore, beneficial both in terms of its effect on drag and on cavitation. Other solutions have been considered and have shown varying degree of effectiveness.

Flow control techniques can be defined as tools to change the natural state of fluid flows and their transition into more controlled and desired flow conditions.²² Flow control strategies are divided into two types: passive and active. Passive solutions include devices that do not rely on the controller or energy sources needed for active control.²³ Passive and active can be effective techniques to manipulate and change wall-bounded or free-shear flows. This change can be made by delaying or inducing advanced transition, suppressing or boosting turbulence, and provoking or suppressing separation. These changes can increase lift, decrease drag, suppress flow-induced noise, and induce

vortex mixing. Devices and structures that can manipulate the fluid dynamics of a system without an external power source include vortex generators (VGs), tailored surface roughness, injection and discharge channels, and surface obstacles as well as grooves to redirect flow and change vortices regime.

Active controls include wall temperature increase, dynamic surface modification by deformation or movable parts, and injection or flow oscillation using blowing, suction, and synthetic jets.²⁴

This article aims to review studies focused on passive flow controls applied to cavitation. Among these, VGs are regarded as the most effective and simplest technique and have been used in many applications such as airfoils, wind turbine blades, swept wing, and heat exchangers.²⁵ Apart from their effectiveness on boundary layer separation, their simple design, low cost, and lower drag make them an effective tool in a broad range of applications.²⁶ Because of this, while other passive flow control technologies are also reviewed, a particular emphasis has been placed on VGs.

The application of passive flow control in compressible external aerodynamics has a significant history. Although there is a noticeable difference between compressible and incompressible flows in the behavior boundary layer separation,²⁷ passive flow control studies in the compressible flow can be a good guide and pattern for incompressible flow cavitation. It is possible to correlate the compressible flow boundary layer behavior to the incompressible flows using three assumptions: (1) the boundary layer is regarded as thermally insulating, (2) the viscosity changes with absolute temperature, and (3) the flow Prandtl number is unity.²⁸ Section II of the article reviews the literature on compressible single-phase flow studies. In Sec. III, different passive flow controls are reviewed in the context of cavitation. Section IV concludes on key results and promising open research topics.

II. PASSIVE FLOW CONTROL TECHNIQUES IN SINGLE-PHASE FLOW

In most aerodynamic applications, such as external flow over aircraft and ground vehicles, and internal flows such as diffusers, boundary layer separation is typically an undesirable phenomenon. Depending on the nature of the wake, separation induces periodic or random pressure variations. Boundary layer separation also leads to

weaker lift, increased drag, and energy losses. Finding ways to control separation and, if possible, prevent it²⁹ is clearly desirable assuming that the applied control method has no impact on efficiency or energy consumption.

The idea of using passive flow control and vortex generation in hydro- or aerodynamic applications is well established and has led to a broad range of studies. Since the late 1990s, several investigations have been focused on the effectiveness of using different passive flow control methods on boundary layer separation and aerodynamic performance.²⁵ According to the analysis of drag coefficients for various Reynolds numbers on a smooth sphere compared to a rough sphere or one with an obstacle, a drag crisis occurs at lower Reynolds numbers, also affecting boundary layer separation (Fig. 1).^{30,31}

The results of these studies guide the implementation of passive control methods in cavitation studies. Vortex generators, distributed roughness, leading-edge slats,^{32,33} flow vanes,³⁴ leading-edge serrations,³⁵ slotted airfoils,³⁶ and suction and blowing techniques^{24,37,38} have all been considered for the application in external aerodynamics.

There is ample evidence that increased surface roughness can be harnessed to induce vortex shedding, insert energy into the boundary layer, and trigger an early transition to turbulence. This has been shown to delay boundary layer separation and increase the extent of the attached flow region.^{39,40} Effects reported include lift recovery and noise reduction.^{41,42} Surface roughness is also effective in postponing stall phenomena and improving an airfoil's aerodynamic performance.⁴⁰

VGs were initially introduced as small aerodynamic devices attached to a part of an aerodynamic vehicle. They are able to generate a small vortex downstream. VGs can have a similar effect transferring momentum from the free stream to the near wall region. They can provide one of the most practical means to control flow separation over airfoils because of their small size.⁴³ Benefits include increased lift, delayed stall, and drag reduction. Most of the published research in this field concentrates on finding a design that optimizes the vortex generators' height, geometry, and location upstream of the separation line. The most important parameters are the geometry, the height, h , the height to pitch ratio, h/δ , the array layout, ΔX_{VG} , l/h , and β . Different VG designs and their important parameters are shown in Fig. 2.

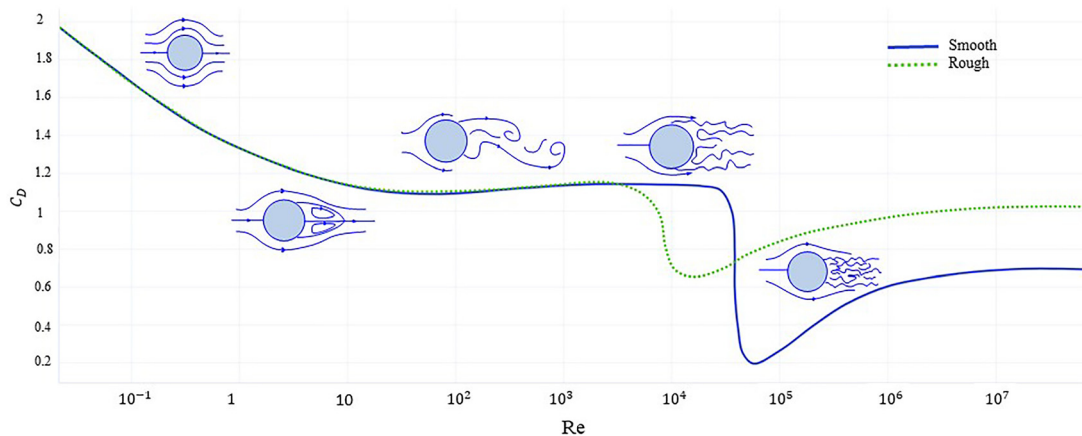


FIG. 1. Dependency of the drag coefficient on the Reynolds number for a smooth and rough sphere.

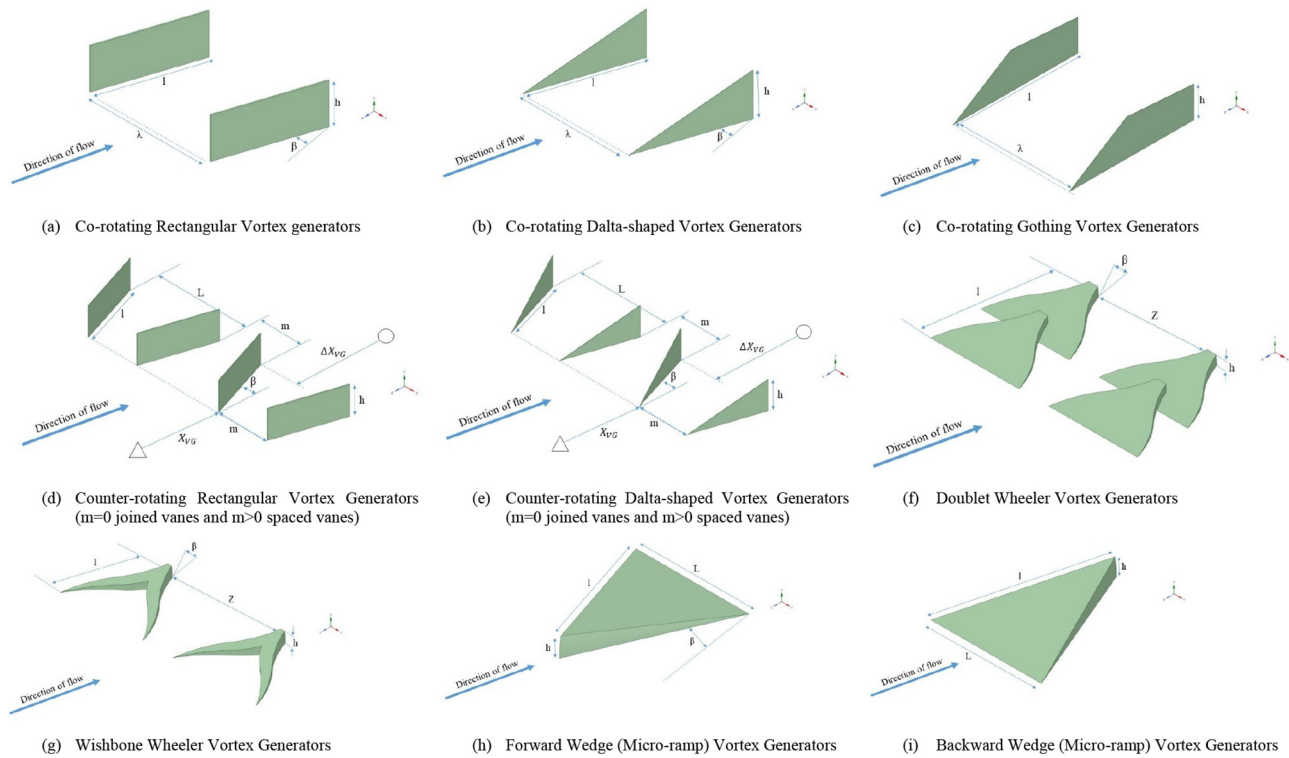


FIG. 2. Schematic of vortex generators with key design parameters, (a) co-rotating rectangular vortex generators, (b) co-rotating delta-shaped vortex generators, (c) co-rotating Gothing vortex generators, (d) counter-rotating rectangular vortex generators ($m = 0$ joined vanes and $m > 0$ spaced vanes), (e) counter-rotating delta-shaped vortex generators ($m = 0$ joined vanes and $m > 0$ spaced vanes), (f) doublet wheeler vortex generators, (g) wishbone wheeler vortex generators, (h) forward wedge (micro-ramp) vortex generators, (i) backward wedge (micro-ramp) vortex generators, which $h =$ device height, $l =$ device chord length, $m =$ vortex generators spacing in the spanwise direction between two pair of counter-rotating vortex generators, $\beta =$ device angle of incidence, $X_{VG} =$ distance between the leading edge and vortex generators, $\Delta X_{VG} =$ distance between the vortex generators trailing edge and baseline separation line, $L =$ distance between two counter-rotating vortex generators' ends, $\lambda =$ distance between two co-rotating vortex generators, and $Z =$ distance between two doublet wheeler or wishbone wheeler vortex generators.

Inducing streamwise instabilities and vortices is one of primary ideas for suppressing the boundary layer separation. In the 1970s, Kuethe⁴⁴ observed a type of centrifugal instability called Taylor–Goertler that can lead to the formation of arrays of streamwise vortices over a concave surface. They tested wave-type VGs and with h/δ in the range 0.27 to 0.42. They observed that VGs caused streamwise vortices in the boundary layer because of a Taylor–Goertler instability. VGs were used to suppress the Kármán vortex stream and to reduce acoustic disturbances in the wake area. They could also confine the velocity deficit region in the wake resulting in improved performance.

Rao and Kariya⁴⁵ investigated so-called submerged VG where the VG height was kept smaller than the boundary layer ($h/\delta \leq 0.625$). A comparison with conventional VGs ($h/\delta \sim 1$) showed that a much lower parasitic drag and better performance in boundary layer separation could be achieved by confining the VG in the boundary layer. Since this seminal work, research has focused on these so-called submerged VGs,^{45–49} which have also been called micro-VGs,^{50–53} sub-boundary-layer VGs,^{54,55} and micro-vanes.⁵⁶ It has been shown, in particular, that VGs with $0.1 \leq h/\delta \leq 0.5$ could provide sufficient momentum transfer toward the wall and over extended downstream region. With a smaller footprint, submerged VGs have also proven to be more versatile for a wider range of applications.

Research on micro-vortex generators (mVGs) has targeted two main research questions; how effective are mVGs at delaying boundary layer separation and what type of vortical flow is generated downstream. A summary is presented in Table I, where studies are classified based on the VGs characteristic parameters such as geometry and location for effective flow control.²⁶

Lin *et al.* conducted important experimental studies on the mVGs effectiveness on boundary layer using a 2D backward-facing curved ramp at low speed at NASA Langley Research Center.^{46,47,49,50} They tested numerous mVGs and other passive flow control methods. Their performance measured in terms of the relative reduction in the extent of the separation region is shown in Fig. 3, with the VG geometries defined in (a), (d), (f), and (g). The most effective methods, such as mVGs and large longitudinal surface grooves, were shown to generate streamwise vortices. mVGs (counter-rotating and co-rotating vane-type VGs with $h/\delta \sim 0.2$ and $h/\delta \sim 0.8$) and Wheeler VGs (wishbone and doublet) were found to have almost the same effects on separation delay. Other methods, such as spanwise cylinders and transverse grooves, generated higher forms of drag and proved less effective.^{47,49,50}

In Fig. 4, visualization of oil flow separation downstream of the baseline surface (without VGs) [Fig. 4(a)] were compared with

TABLE I. Summary of research for effectiveness of micro-vortex generators on boundary layer separation.²⁶

Investigator(s) (year pub.)	Test condition	U_∞^a (m/s)	$Re(Re_\theta^b)$	Mach	δ^c (mm)	VG type	VG parameters					Comments
							h/δ^d	l/h^e	m/h^f	$\beta[\text{deg}]^g$	$\Delta X_{VG}/h^h$	
Lin <i>et al.</i> ⁴⁶ (1990)	Wind-tunnel test low speeds backward-facing ramp	40.2	(9×10^3)	NA	32.5	Doublets	0.1	~13	8	± 25	20	Most effective doublet VGs in separation control: $h/\delta \sim 0.1$.
Lin <i>et al.</i> ^{47,49} (1990–1991)	Wind-tunnel test backward-facing ramp	40.2	(9×10^3)	NA	32.5	Wishbones	0.2	~3	4	± 23	10	Most effective reverse wishbone VGs in separation control: $h/\delta = 0.2$.
Lin ⁵⁰ (1999)	Wind-tunnel test backward-facing ramp	40.2	(9×10^3)	NA	32.5	Counter-rotating rectangular vanes	0.2	4	9	± 25	10	Most effective counter-rotating vanes VGs: $h/\delta \sim 2$. ↑ Embedded streamwise vortices
Ashill <i>et al.</i> ⁵⁵ (2001)	Wind-tunnel test bump	20	19×10^6 (35×10^3)	0.68	33	Counter-rotating delta vanes Forward wedges	0.3	~10	12	± 14	52	Counter-rotating vanes VG with 1 h spacing have more potential for control boundary layer separation.
Ashill <i>et al.</i> ^{54,55} (2001–2002)	Wind-tunnel test and CFD flat plate	10 – 40	NA	NA	60	Counter-rotating vanes	0.5	~10	NA	± 14	15	Vortex strength has been correlated with device Reynolds number.
						Forward wedge	0.5	10	NA	± 14	50	↓ Interference between mutual vortices caused by the spacing between counter-rotating VGs. ↓ Vortices and drag.
						Backward wedge	0.5	10	NA	± 14		
						Single vane	0.5	10	NA	10, 20, 30, 45		
Gorton <i>et al.</i> ⁵¹ (2002)	Wind-tunnel test backward-facing ramp	42.7	NA	NA	22.1	Co-rotating trapezoid vanes	0.2	4	4	23	12 and 9	Most rotating co-rotating trapezoid vanes VGs: Low profile VGs induced a pair of juncture vortices.
Yao <i>et al.</i> ⁵⁷ (2002)	Wind-tunnel test Flat plate	34	NA	NA	35	Single rectangular vane	0.2	0.7	NA	10, 16, 23	100	↑ Embedded streamwise vortex.
Allan <i>et al.</i> ⁵⁸ (2002)	CFD flat plate	34	7.2×10^6	NA	45	Single trapezoid vane	0.2	7	NA	10, 23	15, 27, 52, 102	CFD underestimated the peak vorticity near the VG.
Holden and Babinsky ⁵⁹ (2004)	Wind-tunnel test Backward-facing ramp	NA	28×10^6 (26×10^3)	1.3 and 1.5	1.5	Wedge-type	1	10	12	NA	33	Both type of mVGs effects on the separation bubble under shock and vortex intensity. Vane type mVGs have a strong effect because of strong vortices close to the surface. Wave patterns that result from either mVG contain shocks, re-expansions, and shocks. The pressure losses result in an increase in wave drag.
						Vane-type counter-rotating	0.83	10	12	40		

TABLE I. (Continued.)

Investigator(s) (year pub.)	Test condition	U_∞^a (m/s)	$Re(Re_\theta^b)$	Mach	δ^c (mm)	VG type	VG parameters					Comments
							h/δ^d	l/h^e	m/h^f	$\beta[\text{deg}]^g$	$\Delta X_{VG}/h^h$	
Ghosh <i>et al.</i> , ⁶¹ Babinsky <i>et al.</i> ⁶⁰ (2009–2010)	Wind-tunnel test—blowdown supersonic tunnel	NA	40×10^6	2.5	6.67	Micro-ramps	0.3 – 0.9	7.2	7.5	± 24	13.3 – 16.3	↑The number of counter-rotating streamwise vortices. The largest mVGs have the strongest effect, while it also has the greatest drag. mVGs should be located near the adverse pressure gradients than traditional VGs. Device height is likely to affect optimum location.
Dong <i>et al.</i> ⁶² (2017)	Wind-tunnel test-continuous supersonic tunnel	NA	(3.137×10^4)	1.5	1.125	Slotted ramp-type	1.78	7.2	NA	± 24	21.1	↑Complex wake structure comprised of a confluent counter-rotating streamwise vortex pair and additional streamwise vortices. ↑ Life time, and strengthen the vortex intensity of primary vortex pairs. ↓Generated drag improving the separation control performance.
						Ramp-type	1.78	7.2		± 24	21.1	
Sun <i>et al.</i> ^{66,67} (2019–2020)	Wind-tunnel test	NA	2.3×10^3	5.0	5.17	Micro-ramps	0.25, 0.58, 0.77	7.2	NA	± 24	16.6	↓ Drag and heat flux changing the cortical structures pattern generating spanwise structures, which are caused by the impinging of the arc-like vortices.

^aFree-stream streamwise velocity.^bReynolds number based on momentum thickness.^cBoundary layer thickness.^d h = device height.^e l = Device chord length.^f m = Vortex generators spacing in the spanwise direction.^g β = Device angle of incidence.^h ΔX_{VG} = Distance between the vortex generators trailing edge and baseline separation line.

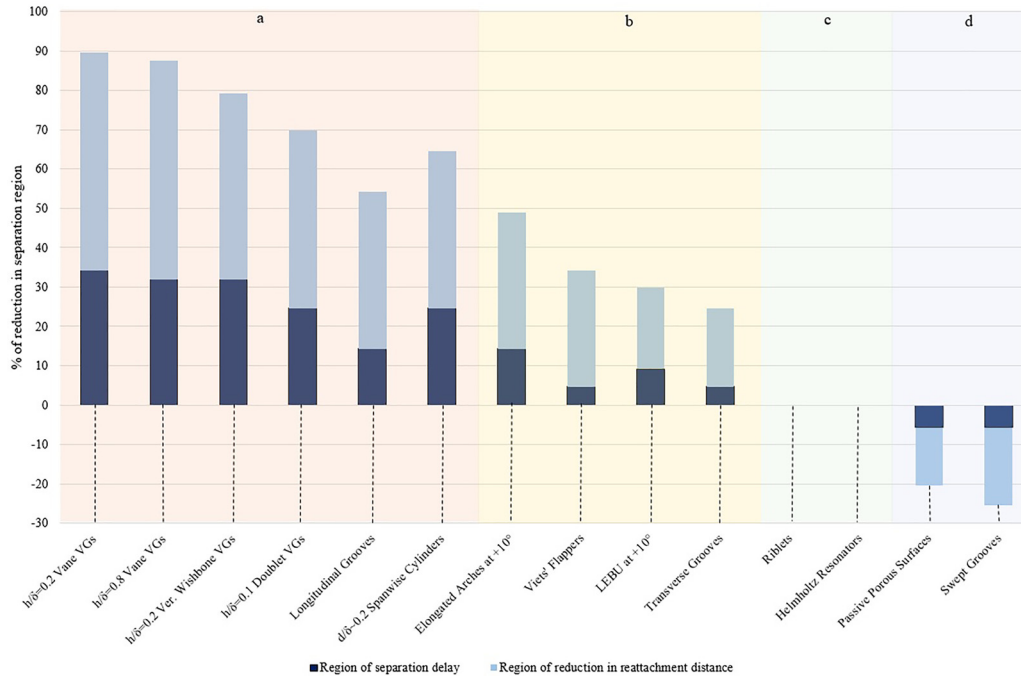


FIG. 3. Effectiveness of micro-vortex generators and other passive flow control methods on the extent of the separation region. (a) A group of devices that generates streamwise vortices and proved most effective at suppressing boundary layer separation; the submerged vortex generators being the most effective and longitudinal producing the lowest effect. (b) Devices that generate transverse vortices, which are still effective; spanwise cylinders and transverse grooves having the highest and lowest effect, respectively. (c) The drag reducing riblets and Helmholtz resonators have no actual effect on boundary layer separation, and (d) passive porous surfaces and swept grooves have the potential to enhance boundary layer separation.⁵⁰

conventional counter-rotating VGs with flow at 6 and 10 h upstream of baseline separation [Figs. 4(b) and 4(c)]. The results of the study found that vortices generated by conventional VGs are stronger than needed and yet are not suppressing separation, while the mVGs achieved close to a 90% reduction in separation and did not generate pockets of recirculating flow. Measurements of surface pressure along

the streamwise direction and at three spanwise locations shown in Fig. 5, clarified the role of mVGs in eliminating separation. Most notable is the lower three-dimensional variability in pressure distribution along the spanwise direction on the shoulder region of the ramp.

Lin *et al.*⁴⁹ examined the impact of further reduction in h/δ from 0.2 to 0.1 and observed a deterioration in the mVG effect on

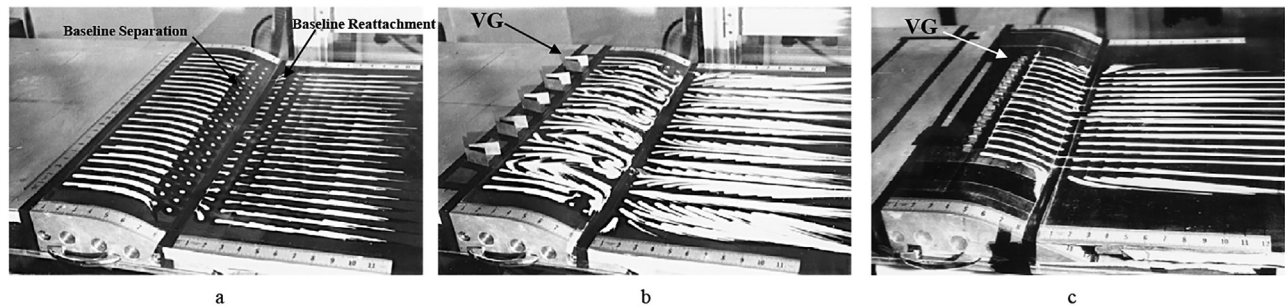


FIG. 4. Oil-flow visualizations of the effect of vortex generators for flows over a backward-facing ramp for the (a) baseline case without vortex generators which produces an obvious two-dimensional separated flow, (b) counter-rotating conventional vane-type vortex generators ($h/\delta \sim 0.8$) placed 5δ upstream of a baseline separation which could produce an attached flow downstream of the ramp albeit with strong three-dimensional features including a visible recirculation zone downstream of the separation baseline, (c) vane-type counter-rotating vortex generators ($h/\delta \sim 0.2$) placed at 2δ upstream of baseline separation which could suppress the boundary layer sufficiently with lower three-dimensional variations in the spanwise pressure at the shoulder region of the ramp.⁵⁰ From Lin, *Control of Turbulent Boundary-Layer Separation Using Micro-Vortex Generators*. Copyright 1999 American Institute of Aeronautics and Astronautics, Inc. Reprinted with permission from American Institute of Aeronautics and Astronautics, Inc.

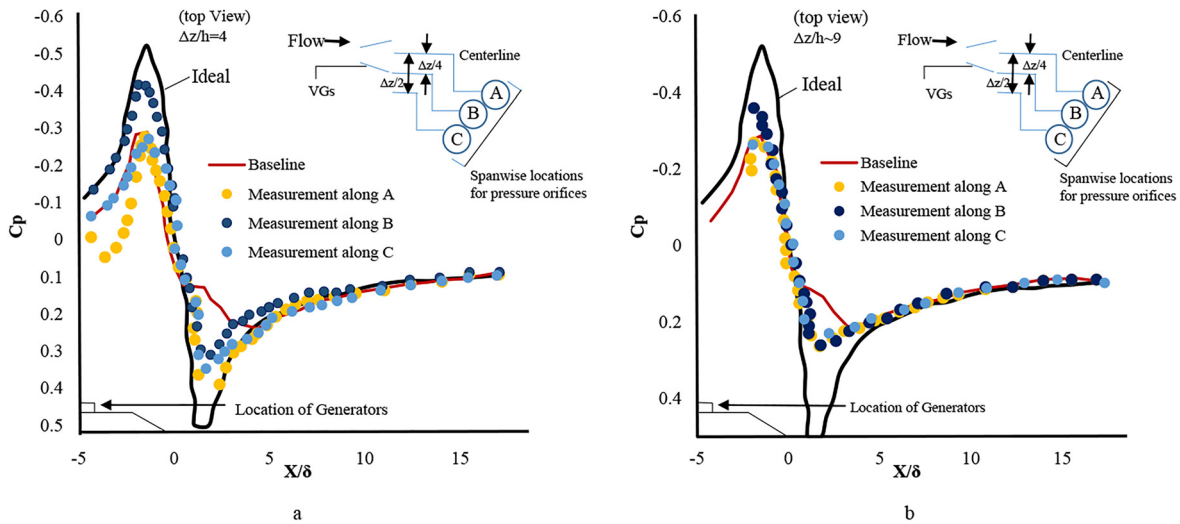


FIG. 5. Spanwise variations in the streamwise pressure distribution with (a) conventional vane-type counter-rotating vortex generators ($h/\delta \sim 0.8$) placed at 5δ upstream of baseline separation, which shows noticeable differences between the three spanwise positions, (b) counter-rotating vane-type micro-vortex generators placed 2δ upstream of the baseline separation, which show a lower spanwise pressure variation compared to conventional vortex generators.⁵⁰ From Lin, *Control of Turbulent Boundary-Layer Separation Using Micro-Vortex Generators*. Copyright 1999 American Institute of Aeronautics and Astronautics, Inc. Reprinted with permission from American Institute of Aeronautics and Astronautics, Inc.

separation. These results confirmed that mVGs can be more effective in controlling flow separation than larger VG but care must be taken in determining an effective height to boundary layer thickness ratio to avoid.

Ashill *et al.*⁵⁵ performed a comparative study on wedge type and counter-rotating mVGs located $52h$ upstream of the baseline separation line. The counter-rotating mVGs [Fig. 2(e)] with a $1h$ spanwise gap proved most effective at suppressing boundary layer separation.

Gorton *et al.*⁵¹ studied the effects of mVG profile changes (Fig. 6) in suppressing separation from a backward-facing ramp with co-rotating Goring VGs [Fig. 2(c)]. The study relied on oil-flow

visualization illustrated in Fig. 7. Figure 7(a) shows two large spiral nodes and a central reverse flow at the ramp in the baseline case. The mVGs proposed by Gorton *et al.*⁵¹ with $h/\delta \sim 0.2$ is shown in Fig. 7(b) to alter the direction of near-wall flow sufficiently to suppress separation.

Ashill *et al.*^{54,55} also studied the flow characteristics of mVGs at the UK Defense Evaluation Research Agency Boundary Layer Tunnel. They performed tests for a range of mVGs with $h/\delta \sim 0.5$, including the single vane, counter-rotating vane-type, forwards, and backward wedges shown in Fig. 2. The generated vortex strength was estimated from flow field measurements using a laser doppler anemometer up to

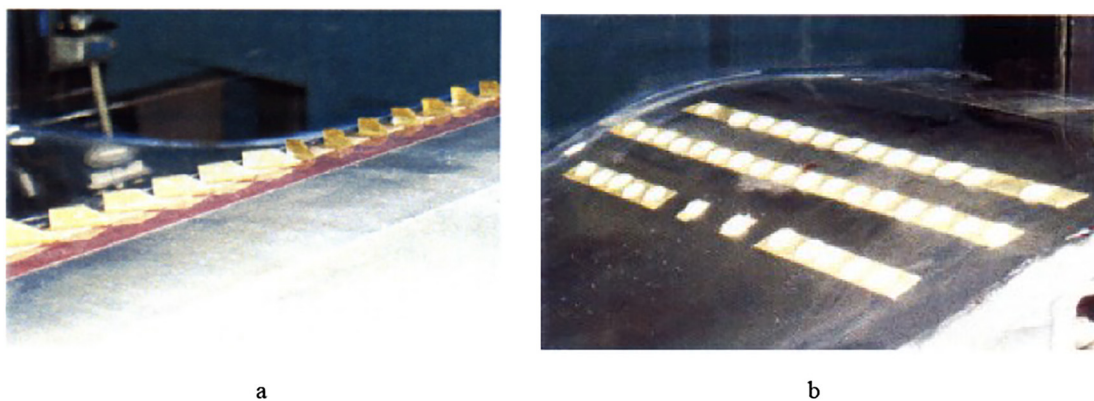


FIG. 6. (a) Co-rotating Goring micro-vortex generators configured at an angle of 23° to the onset flow were created by Gorton *et al.*,⁵¹ which resulted in significant pressure gradient reduction and (b) installation of micro-bump arrays on the ramp with a maximum height of 10% of the boundary layer thickness.⁵¹ From Gorton *et al.*, *Flow Control Device Evaluation for an Internal Flow With an Adverse Pressure Gradient*. Copyright 2002 American Institute of Aeronautics and Astronautics, Inc. Reprinted with permission from American Institute of Aeronautics and Astronautics, Inc.

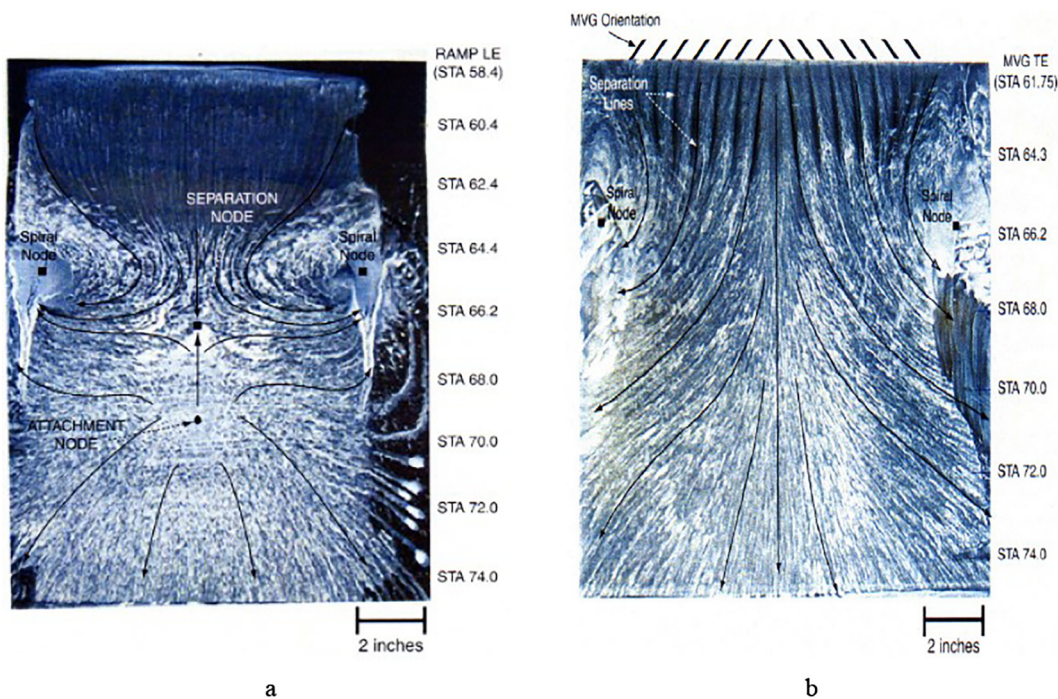


FIG. 7. (a) Oil flow visualization of baseline case for flow over a backward-facing ramp with vortex generators and at an onset velocity of 42.7 m/s. The image provides evidence of large spiral nodes and a central reverse flow. (b) Oil flow visualization of the effect of vane-type co-rotating Goring micro-vortex generators with $h/\delta \sim 0.2$ in comparison with the baseline case using which direction change of near wall flow and suppressing reversing flow is shown.⁵¹ From Gorton *et al.*, *Flow Control Device Evaluation for an Internal Flow With an Adverse Pressure Gradient*. Copyright 2002 American Institute of Aeronautics and Astronautics, Inc. Reprinted with permission from American Institute of Aeronautics and Astronautics, Inc.

15h downstream of the mVGs⁵⁵ and up to 50h downstream of the mVGs.⁵⁴ They proposed a correlation for the non-dimensional circulation and used the concept of a mVG sufficient height.⁵⁵ The correlation provides a prediction of the VG vortex strength downstream and is applicable for a wide range of Reynolds numbers. No relation is provided, however, between the sufficient height and a physical dimension of the mVGs. The study found that forwards-wedges and the joint-vane mVG create counter-rotating vortices sharing a mutual interface.⁵⁵ Measurements indicated that this led to reduced vortex strength. The vortices generated by backward wedge mVGs were found to be always closer to the wall impacting on wall shear.

Counter-rotating vane mVGs were shown to double the vortex strength when tested up to 50 h downstream of the mVGs. The joined-vane and the forwards-wedge mVGs produced stronger vortex decay than the two 1 and 2 h spaced counter-rotating vanes mVGs at a downstream distance of up to 15 h. In terms of adverse pressure gradient, spaced vanes proved to be more efficient than joined vanes. In comparison to counter-rotating vanes, forward-wedge mVGs reduced drag by 60%. According to the analysis of counter-rotating vanes, increasing the gap ratio can help decrease the generated drag of devices.

In other studies, Yao *et al.*⁵⁷ and Allan *et al.*⁵⁸ conducted an experimental and numerical analysis of single vane-type mVGs on a flat plate. A flow field measurement system was developed to characterize embedded streamwise vortices downstream of mVGs. Their

system consisted of a 3D stereo-imaging and particle image velocimetry (PIV) system covered downstream vane-type mVGs. CFD and experimental results both demonstrated that downstream of mVGs, vortices decay substantially regardless of the device incidence angle.

The effectiveness of wedge-shaped and counter-rotating vane mVGs interaction with shocks and boundary layer at Mach numbers of 1.5 and 1.3, was also investigated by Holden and Babinsky.⁵⁹ They observed that both types of mVGs affected the separation bubble under shock and the vortex intensity. Although the vane type mVGs were shown to have a stronger effect because of the higher vortex strength closer to the surface, both types of mVGs can create a wave pattern consisting of shocks, re-expansions, and shocks. Wave drag and pressure losses increase due to this pattern. It was also observed that wedge-shaped mVGs generated vortices that lifted off the surface more quickly.

Babinsky *et al.*⁶⁰ and Ghosh *et al.*⁶¹ conducted experimental and CFD analyses of forward wedge type mVG. The formation and evolution of multiple pairs of counter-rotating streamwise vortices were observed downstream of the mVGs as shown in Fig. 8. A low-momentum region forms in the wake of the wedge along the centerline between consecutive mVGs. The magnitude of momentum deficit was found to be proportional to the size of mVGs and inversely proportional to the drag induced by wedge-type while the two counter-rotating vortices act to transfer high momentum from the boundary layer peripheral region to the surface. Despite the strongest effects and

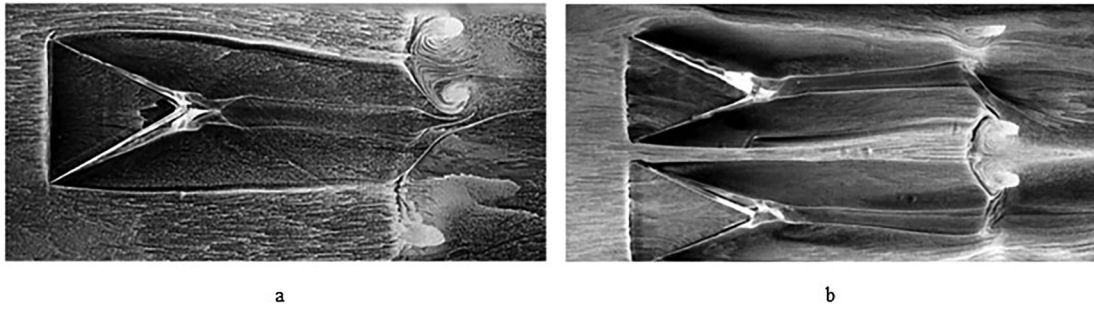


FIG. 8. A surface oil-flow visualization for flow over micro-ramp developed by Babinsky *et al.*⁶⁰ Implementation of micro-ramps generate a region of attached flow in its immediate downstream centerline and break down the overall separation region into small individual separation areas. The generation of streamwise vortex pairs is shown to develop in both individuals and array of micro-ramps. Reprinted by permission Babinsky *et al.*, *AIAA J.* **47**, 668 (2009).⁶⁰ Copyright 2009 American Institute of Aeronautics and Astronautics, Inc.

greatest drag caused by the largest mVGs, the smallest mVGs ($h/\delta = 0.3$) had similar effects on separation with lower induced drag. The results also indicated that mVGs should be located closer to the adverse pressure gradients region than traditional VGs.

Dong *et al.*⁶² proposed a new slotted ramp-type mVGs and numerically investigated their effect on the flow separation in supersonic flow. A more complicated wake structure was observed, including two confluent counter-rotating streamwise vortices and an increase in number of streamwise vortices. The interaction of these vortices with the primary counter-rotating vortex pair could increase the lifetime of vortices and boost the vortex intensity. These slotted mVGs also decrease the generated drag compared to standard micro-ramps and improve the separation control performance.

Sun *et al.*⁶³ developed a conceptual description of the evolution of the vortical structures in the wake of the micro-ramps in supersonic

flows as illustrated in Fig. 9. Based on Li and Liu⁶⁴ and Sun *et al.*,⁶⁵ velocity shear and, consequently, pressure gradients downstream of micro-ramps induce swirling vortices in an arc or ring shape. The mechanism of vortex generation can be linked to Kelvin–Helmholtz (K–H) instabilities. The model of Sun *et al.*⁶³ depicts the dynamics of vortices in stages of K–H evolution. Initially, the streamwise vortices generated as focused filaments which quickly lose their stability and change into arch-shape K–H vortices. The wavelength of the instability starts to increase due to shear velocity and vortex pairing increase. As the legs of the arch-shaped K–H vortices grow and merge with neighboring vortices, vortex rings are eventually formed. As a result of streamwise vortices, downward motion is induced at this stage. Turbulent distortion eventually causes the ring vortices to break down.

Sun *et al.*^{66,67} also conducted a numerical modeling to analyze the wake of micro-ramp VGs under hypersonic conditions. They

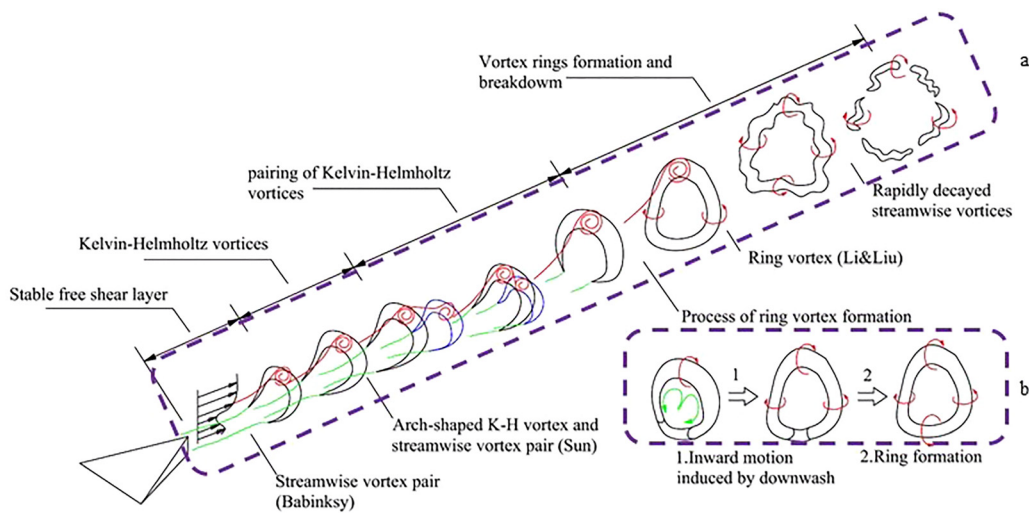


FIG. 9. Conceptual model of vortical structures created by micro-ramps.⁶³ (a) The streamwise vortex pairs are initially generated immediately downstream of the micro-ramp. As a result of the instability of the curved free shear layer around the wake, these vortices developed into arch-shaped Kelvin–Helmholtz vortices. Kelvin–Helmholtz vortices pair with each other, and mean shear velocity increases which cause the instability wavelength to increase. Kelvin–Helmholtz vortex rings are formed by the leg portions of arch-shaped vortices extending to the bottom side of the turbulent wake. These vortex rings break down downstream as a result of turbulent distortion. (b) Process of vortex ring formation. Republished with permission of Sun *et al.*, *Phys. Fluids* **26**, 025115 (2014). Copyright 2014 Clearance Center, Inc.

observed a type of arch-type vortices that grow moving downstream and breaking the primary vortices. They found that these mVGs can generate spanwise structures caused by the impinging of the arc-like vortices. Their result showed that drag and heat flux were reduced after applying mVGs to change the cortical structure pattern.

Other applications of passive control in compressible flows not in the scope of this article are reviewed in detail by Akhter and Omar⁶⁸ and Genç *et al.*²⁵

As a conclusion of this section, the results show that mVGs can effectively control flow separation over airfoils. The most important effects relate to boundary layer separation. The generation of streamwise vortices in the boundary layer, transfers momentum toward near the wall, delaying and suppressing boundary layer separation, increasing lift, and decreasing drag and pressure recovery downstream of VGs. The mVGs are quite efficient in suppressing shock-induced separation in supersonic flow and reducing the reverse flow region. The highest effectiveness has been observed in cases with fixed boundary layer separation by locating the VG closer than $100h$ distance upstream of baseline separation.

The geometry and arrangement of mVGs are critical parameters. The best performances have generally been reported with $0.2 < h/\delta < 0.5$, but effective flow separation is still possible with $0.1 < h/\delta < 0.2$. The counter-rotating mVGs have demonstrated better

efficiency in 2D flow separation tests, whereas co-rotating mVGs have been found more effective in 3D separation tests. From the literature reviewed here, the most effective distance between the upstream mVGs and the baseline separation is in the range of $5h$ to $30h$.

III. PASSIVE FLOW CONTROL STUDIES IN CAVITATION

In this section, we focus on passive techniques to control cavitation. Several methods, including geometry modification, injection, drainage, surface conditioning, obstacles, grooves, and VGs, have been proposed to attempt to passively control the boundary layer and cavitation instability effects. Table II summarizes the different types of cavitation to understand better the analyses reviewed in this article. Sections III A–III F present a review of studies of these different methods and their effects on cavitation. The summary overview of the methods and key results are presented in Table III–Table V.

A. Surface condition and roughness

The properties of a solid surface, coatings, and roughness influence boundary layers, affecting heat transfer and momentum transfer through the fluid–surface interface and influencing cavitation. The boundary layer flow over smooth and rough surfaces is shown in Fig. 10.

TABLE II. A brief definition of different type of cavitation with schematics and experimental observations. (a) Reprinted with permission from Chen *et al.*, Acta Mech. Sin. 36, 1202 (2020). Copyright 2020 Springer Nature Customer Service Center GmbH. (b) and (d)–(g) Courtesy of Grenoble Univ.⁶⁹ (c) Reprinted with permission from De La Torre *et al.*, J. Fluids Struct. 39, 173–187 (2013). Copyright 2013 Elsevier.

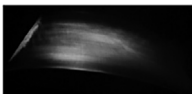
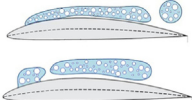
Cavitation regime	Definition and characterization	Schematic	Experimental observation ^{69–71}
(a) Incipient cavitation	Beginning stage of cavitation where pressure reaches a level at or below saturation pressure and nuclei sites start to grow		
(b) Traveling bubble cavitation	Growth and collapse of isolated bubbles close to the surface		
(c) Attached or sheet cavitation	Large-scale cavitation structures that form as a result of the transition from traveling bubble cavitation to one vapor-filled wake		
(d) Partial cavity	An attached cavity which covers only a part of the foil		
(e) Cloud cavitation	A shedding cavity that develops when a reentrant jet emerges from the closure region of the attached cavity and sheds by an unsteady partial cavity		
(f) Super-cavity	An attached cavity that extends over the entire suction side of the foil and closes downstream of the foil trailing edge		
(g) Tip vortex cavitation	Due to the rotating motion, the static pressure at the center of vortices drops much lower than that in the freestream, resulting in a swirling cavitation stream		

TABLE III. Summary of research for implementing roughness as a surface methodology technique in cavitation control.

Investigator(s) (year)	Type of modification	U_{∞}^a (Re)	α^b	σ^c	Coating roughness	Cavitation regime	Comments
Coutier-Delgosha <i>et al.</i> ⁷⁶ (2005)	Wall roughness on a two-dimensional foil ($c^d = 150$ mm, $S^e = 80$ mm)	6 m/s	$0^\circ - 6^\circ$	0.7 – 1.8	100, 200, 400 μm	Cyclic cloud sheet cavitation	<ul style="list-style-type: none"> ↓ Cavity length ↑ Oscillation frequency ↓ Pressure fluctuation intensity
Ausoni <i>et al.</i> ^{77,78} (2007 and 2012)	Blunt trailing edge on NACA 0009 hydrofoil ($c = 100$ mm, $S = 150$ mm)	$(16.1 \times 10^3$ $-96.6 \times 10^3)$ $(42 \times 10^3$ $-70 \times 10^3)$	0°	NA	125 μm ($\frac{\Delta X}{c} = 4\%$) Width = 4%	Vortex shedding	<ul style="list-style-type: none"> ↑ Organized vortex shedding ↓ vortex shedding frequency ↑ Vortex spanwise organization ↑ Vibrations induced by vortices ↑ Vortex strength and wake velocity fluctuations generates many tiny bubbles, which may be erosive in turbomachines
Onishi <i>et al.</i> ⁸⁴ (2017)	Hydrophilic and hydrophobic coatings on symmetrical NACA16 – 021 ($c = 40$ mm, $S = 60$ mm)	3 m/s (1.1×10^5), 5 m/s (2.0×10^5)	$10^\circ, 14^\circ, 20^\circ$	0 – 4.5	3 – 4 μm	Tip vortex cavitation, sheet cavitation, and cloud cavitation	<ul style="list-style-type: none"> ↓ Incipient cavitation number ↓ Cavitation growing for in hydrophilic coating Losing functionality after 210 s of cavitation condition for both hydrophilic and hydrophobic coatings
Hao <i>et al.</i> ⁸⁵ (2018)	Surface roughness on Clark-Y hydrofoils ($c = 70$ mm)	8 m/s (5.6×10^5)	8°	0.87, 1.02	6.9 μm	Cyclic cloud	<ul style="list-style-type: none"> Change in the development of cloud cavitation ↑ Intensity of cavitating flow around the rough hydrofoil
Chen <i>et al.</i> ⁷⁰ (2020)	Surface roughness on NACA 66 hydrofoil ($c = 100$ mm, $S = 149$ mm)	6 – 14 m/s ($0.6 - 1.4 \times 10^6$)	$-12 - 12^\circ$	1 – 5.5	150 μm . ($\frac{\Delta X}{c} = 4\%$) Width = 4%	Inception sheet cloud	<ul style="list-style-type: none"> ↑ Lift, drag and lift to drag ratio ↑ Minimum pressure coefficient No effect on cloud cavitation formation
Svennberg <i>et al.</i> ⁸⁷ (2020)	Uniform and non-uniform roughness patterns on elliptical foil ($c = 126.5$ mm, $S = 300$ mm)	6.8 m/s (8.95×10^5)	9°	NA	$h = 230 \mu\text{m}$	Tip vortex cavitation	<ul style="list-style-type: none"> ↓ Cavitation number for tip vortex cavitation inception ↑ Drag force ↑ Nano- and micro-sized residual air pockets

^aFree-stream streamwise velocity.^bAngle of attack.^cCavitation number.^dHydrofoil chord.^eHydrofoil Span.

TABLE IV. Summary of research for blade profile and geometry modification, drainage and injection, and grooves and slits as surface methodology techniques in cavitation control.

Investigator(s)	Type of modification	$U_\infty (Re)$	α	σ	Geometry properties	Cavitation regime	Comments
Blade profile and geometry modification							
Custodio <i>et al.</i> ¹³⁸ (2018)	Protuberances on the hump-back sinusoidal pattern on NACA 634-021 profile (c = 200 mm)	7.2 m/s (7.2×10^5)	-12° -30°	σ_{in} = 0 – 9	Protuberances amplitude = 0.025, 0.05, and 0.12 c; protuberances wavelength: 0.25, 0.5 c	Sheet cavitation	Confining the cavitation to the region behind the protuberance with medium and large protuberance amplitudes Improving the sheet cavitation pattern.
Zhao and Wang ¹³⁹ (2019)	Bionic fin–fin structure on 2D NACA-0015 (c = 100 mm, S = 100 mm)	10 m/s (1×10^6)	8°	0.8	Rectangular fins, width = 2 % c distance of the two symmetric structures = 20% c, the inclination angle is 14; front distance of the symmetrical structure is 50%	Cyclic cavitation	↓ Turbulent kinetic energy of the hydrofoil ↑ Lift-to-drag ratio
Petkovšek <i>et al.</i> (2018) ⁸⁰	Laser-textured surfaces on stainless steel cylinders (diameter = 10 mm)	Flow rate: 163 – 231 L/s	NA	1.2 – 2.2	Micro-channels width: 100 μm four different angles (0° , 18° , 45° , 72°); distance between channels: 200 and 500 μm ; micro-holes: diameter: 40 μm ; distance between holes: 200 μm	NA	↓ Cavitation extent ↓ Cavitation incipient number
Kant and Bhattacharyya ¹⁴⁰ (2020)	Twin-protuberance NACA 634-021 hydrofoil (c = 100 mm, S = 200 mm)	2 m/s (2×10^5)	$5-25^\circ$	NA	Twin-protuberance hydrofoil design mimicking the two prominent tubercles present on a humpback whale flipper	NA	Limit the separation zone between the chordwise vortices shed from the two humps at high angles of attack ($>20^\circ$). ↓ Pre-stall lift coefficient ↓ Stall separation, ↑ Lift after stall. Effectively control flow at high angles of attack
Li <i>et al.</i> ¹⁴¹ (2021)	Bionic NACA 634-021 hydrofoil with a wavy leading-edge (c = 102 mm, S = 204 mm)	7.2 m/s (7.2×10^5)	18°	NA	Design inspired from pectoral fin of humpback whales, sinusoidal with amplitude = 0.05c, and wavelength = 0.5c	Attached cavitation; cloud cavitation	↑ Improves lift–drag characteristics ↓ Cavitation volume by around ↓ Pressure amplitude Enhances cavitation suppression Restrains hydrofoil cavitation
Drainage and injection							
Arndt <i>et al.</i> ¹⁵² (1995)	Air injection on NACA 0015 (c = 81 mm, half S = 95 mm)	20 m/s	8°	0.5 – 6	5 holes with 5 mm distance from each other and 0.5 mm diameter	Sheet cavitation	Effectively minimizes cavitation erosion
Zhu <i>et al.</i> ¹⁵⁴ (2014); Bin <i>et al.</i> ¹⁵⁵ (2016)	Gap impeller on pump's blades (Cylindrical 2D blades for a LSSCP)	$17.3 \frac{\text{m}}{\text{s}}$ (45×10^3)	NA	0 – 1	Pump: 4 gad; impellers rotating speed = 1000 rpm; water head = 7 m	Cloud cavitation	↑ Pump's hydraulic performance and cavitation resistance Suppressing generating cavitation A new cavitation regime with different attack angles was developed; allocated flow discharge and cavitation volume affects this new cavitation structure

TABLE IV. (Continued.)

Investigator(s)	Type of modification	$U_\infty(Re)$	α	σ	Geometry properties	Cavitation regime	Comments
Wang <i>et al.</i> ¹⁵⁷ (2017)	Water injection on NACA0066 hydrofoil (c = 150 mm)	5.33 m/s (0.8×10^6)	6, 8°	0.55 – 1.0	Jet hole diameter: 2 mm; injection position: 10–90 %c	Cloud cavitation	Water injection angle and jet angle affect cavitation suppression ↑ Boundary layer velocity gradient enhances anti-reverse pressure gradient ↓ Recirculation zone thickness ↓ Velocity of the re-entrant jet ↓ Intensity of separation flow ↓ Cavity volume
Kamikura <i>et al.</i> ¹⁵⁶ (2019)	Asymmetric slits on each blade of Inducer 335	NA	NA	0.01 – 0.3	Slit depth 30 mm; slit width 5 mm; inducer speed = 6000 rpm	Vortex cavitation	Suppressing cavitation instabilities by rearranging the asymmetric slits
Groove and slit Li <i>et al.</i> ¹⁴⁶ (2009)	Distributed grooves on MK46 torpedo (c = 120 mm)	25 – 30 m/s	NA	NA	Groove width: 3–10.5 mm; groove depth: 1.5 mm; number of grooves: 9–28	Cyclic cloud	The effect on the cavity clouds' position and shape depends on grooves' dimensions ↑ Pressure fluctuation ↑ Pressure drops in certain local regions, which may increase the possibility of enhanced cavitation inception ↓ The stability of the cavities because of pressure fluctuation
Danos <i>et al.</i> ^{147,148} (2014)	Longitudinal grooved surfaces on a Venturi	~8 m/s ($5.2, 5.5 \times 10^5$)	NA	1 – 1.8	D = 1, 2 mm; h = 0.25, 2 mm; N = 40–124	Sheet cavitation Cloud cavitation	↓ Shedding of unsteady partial cavitation ↓ Surface erosion Suppressing the cloud cavitation shedding Groove geometries affect cavitation regimes One of the determining factors is the depth of grooves Large depth of grooves can modify the sheet cavity structure No change in the sheet cavity length with groove's depth smaller than viscous sublayer thickness
Cheng <i>et al.</i> ¹⁵⁰ (2020)	Overhanging grooves attached to the f d NACA0009 hydrofoil tip (c = 100 mm)	10 m/s	10°	2	Attaching several tabs, connected with each other by a slender beam with gap of 2, 7, and 20 mm	Tip-leakage vortex	More suppression for small gaps OHGs with small gap sizes can weaken the strength of both TLV and tip-separation vortex ↑ In the TLV core size ↑ Local minimum pressure limiting influence on the performances of hydrofoil in a large range of the gap sizes

TABLE V. Summary of research for obstacles and vortex generators studies in cavitation control.

Investigator(s)	Type of modification	U_∞ (Re)	α (°)	σ	h (mm) (h/δ)	$\Delta X_{VG}/c$ ($\Delta z/c$)	Cavitation regime	Comments
Obstacles								
Kawanami <i>et al.</i> ¹⁵⁸ (1997)	An obstacle on an elliptic nose foil ($c = 150$ mm and $S = 150$ mm)	Propeller tunnel 5.0 m/s (7.2×10^5); for TE tunnel $7.5 \frac{m}{s}$ (8.6×10^5)	6	Propeller tunnel: 1.07 TE tunnel: 1.72	2 (width 2 mm)	37% c 60% c	Cyclic cloud	Holding back the re-entrant jets ↓ Cloud cavitation ↓ Noise intensity ↓ Cavitation drag coefficient
Pham <i>et al.</i> ¹⁵⁹ (1999)	Obstacle on the flat ($c = 150$ mm, $S = 80$ mm)	8 m/s (1.2×10^6)	3, 3.25, 3.5	0.94	2 (width 4 mm)	23.3% c	Cyclic cloud	Cloud cavitation control Holding back re-entrant jets
Sato <i>et al.</i> ¹⁶⁰ (2002)	Obstacle on the flat hydrofoil ($c = 70$ mm, $S = 70$ mm)	3.59 m/s	3.8	0.8, 1.0	3 (width 3 mm)	33% c	Cyclic cloud	No change in the frequency or magnitude of oscillation
Zhao <i>et al.</i> ¹⁶¹ (2010)	Obstacle on the NACA0015 hydrofoil ($c = 100$ mm)	(1×10^6)	8	1.2, 1.5	1, 2 (width 2 mm)	32%, 37%, 45% c	Cyclic cloud	↓ Lift and drag force ↑ Lift to drag ratio ↓ Cloud cavitation Restraining re-entrant jets
Ganesh <i>et al.</i> ¹⁶² (2015)	Venturi wedge ($c = 241.3$ mm, $S = 76$ mm)	8 m/s	22.1	1.81 – 1.94	4 (width 4 mm)	26.1% c	Cyclic cloud	↓ Void fraction in the cavity ↑ Cavity length
Zhang <i>et al.</i> ¹⁶⁸ (2018)	Obstacle on the flat hydrofoil ($c = 150$ mm, $S = 200$ mm)	10 m/s	0	0.68 – 0.76	2 (width 2 mm)	37% c	Shedding cavitation Cloud cavitation	Constant average cavity length Changing the transient re-entrant jets in terms of strength and direction
Che <i>et al.</i> ¹⁶⁷ (2019)	Spanwise obstacle on the 2D NACA0015 hydrofoil ($c = 100$ mm, $S = 200$)	6 m/s	6.5 – 8	0.8 – 1.7	2 (width 2 mm)	25%, 30.7%, 39%, 47.3%, 53% c	Sheet cavitation Shear cavitation	↓ Sheet cavitation ↑ Pressure in the near-wall region ↓ Energy flux, cavity length, and acoustic intensity Cloud cavitation control Cannot suppress cavitation under transitional cavity oscillation
Lin <i>et al.</i> ¹⁷⁰ (2021)	Different-sized arc obstacles on a flat hydrofoil ($c = 100$ mm)	14 m/s	5	1	Convexity of the arc = radius/ $5 = 1$ –2.4 mm	NA	Cloud cavitation	↓ Shedding cavity size ↑ Shedding frequency as arc radius increases Stabilize the frequency of shedding cavity on the leading edge Transforming the large-scale shedding to the small-scale shedding at the trailing edge as arc radius increases

TABLE V. (Continued.)

Investigator(s)	Type of modification	U_∞ (Re)	α (°)	σ	h (mm) (h/δ)	$\Delta X_{VG}/c$ ($\Delta z/c$)	Cavitation regime	Comments
Vortex generators								
Javadi <i>et al.</i> ¹⁷⁴ (2017)	Artificial cavitation bubble generator on hydrofoil CAV2003 ($c = 100$ mm)	6 m/s	7°	0.4 – 4	0.367 mm	NA	Periodic cloud shedding	<ul style="list-style-type: none"> ↓ Lift and drag fluctuations Producing low-pressure recirculating area Inducing stationary cavitation bubbles Controlling parameters: the location, shape, and size of VGs are the crucial
Kadivar <i>et al.</i> ¹⁷⁷ (2018)	Wedge-type cavitating bubble generators on CAV2003 benchmark hydrofoil ($c = 100$ mm)	6 m/s (6×10^5)	7°	0.8	0.25 – 0.3 mm (width 0.75% –1.1% c)	0.6% –21.3% c	Cyclic cloud	<ul style="list-style-type: none"> ↑ Kinematic energy in the near-wall surface withstanding a pressure rise before the separation ↓ Quick surface high-pressure pulsations ↓ Cyclic behavior of unsteady cloud cavitation ↓ Turbulent velocity fluctuation transferring high momentum fluid into the vicinity of the wall surface Changing vortex structures and the hydrofoil wake region
Kadivar <i>et al.</i> ¹⁸¹ (2019)	Cylindrical cavitating bubble generators on CAV2003 benchmark hydrofoil ($c = 100$ mm)	6 m/s (6×10^5)	7°	0.8	0.25 – 0.3 mm ($D = 1.1\%$ –4% c)	6% – 66% c (1% c)	Cyclic cloud	<ul style="list-style-type: none"> ↓ Adverse pressure gradient at the closure region of cavity ↓ Re-entry jet strength ↓ Cavitation-induced vibration ↓ Near surface high pressure picks Mitigation of cloud cavitation instabilities
Kadivar <i>et al.</i> ¹⁸² (2019)	Cylindrical cavitating bubble generators on CAV2003 benchmark hydrofoil ($c = 100$ mm)	(1.4 – 1.5 $\times 10^6$)	NA	NA	1 mm ($D = 1$ mm)	36% (4%)	Cyclic cloud	<ul style="list-style-type: none"> ↓ Large-scale cavitation clouds ↓ Pressure pulsations at the wake region Shedding happened only in small-scale cavity

TABLE V. (Continued.)

Investigator(s)	Type of modification	U_∞ (Re)	α (°)	σ	h (mm) (h/δ)	$\Delta X_{VG}/c$ ($\Delta z/c$)	Cavitation regime	Comments
Che <i>et al.</i> ^{171,184,186} (2017–2019)	Delta-shaped counter-rotating VGs on NACA0015 hydrofoil ($c = 100$, $S = 200$ mm)	7 m/s (0.6×10^6)	$6.5^\circ - 8^\circ$	0.8 – .7	0.05 – 0.25 mm (0.5 – 2.5) ($l = 0.4$ mm, $\beta = 18^\circ$)	2.5%	Sheet cavitation	<ul style="list-style-type: none"> ↑ Momentum transfer toward the surface ↑ Cavitation length ↓ Dominant frequency of cavitation (TCO and PCO condition) ↑ Vortex cavitation length by decreasing the height of mVGs ↓ Flow disturbance in the spanwise direction Suppression of boundary layer separation Induce inception of vortex cavitation Cavity moving toward leading-edge Vanishing classical fingering structures and Tollmien–Schlichting waves Creating a uniform sheet cavity in the spanwise direction Suppressing R-T and K-H instabilities
Kadivar <i>et al.</i> ¹⁷⁸ (2020)	Wedge-type cavitating bubble generators on CAV2003 benchmark hydrofoil ($c = 100$ mm)	(1.1×10^6 -1.6×10^6)	$5^\circ, 7^\circ, 11^\circ$	0.66 – 1.3	NA	NA	Cyclic cloud	<ul style="list-style-type: none"> ↓ Amplitude of pressure pulsations Hampering a reentrant jet Hindering cloud cavities
Qiu <i>et al.</i> ¹⁸⁷ (2020)	Delta-shaped counter-rotating VGs on NACA0015 hydrofoil ($c = 100$, $S = 200$ mm)	10 m/s (1.37×10^6)	6.5, 8	1.35 and 1.7	0.25 mm (2.5) ($l = 0.4$, $\beta = 18^\circ$)	2.5%	Attached cavitation	<ul style="list-style-type: none"> New cavitation structure including vortex cavitation-transition region-attached cavitation Not possible to delay or suppress the attached cavitation in these conditions More stable sheet cavitation More shedding in cloud cavity
Huang <i>et al.</i> ¹⁸⁸ (2020)	VGs on ship propeller	14.37 m/s	0 – 45	0.291 6	20 mm	NA	Sheet cavitation	<ul style="list-style-type: none"> ↓ Pressure fluctuation ↓ Cavitation instability Inducing more uniform wake

TABLE V. (Continued.)

Investigator(s)	Type of modification	U_∞ (Re)	α (°)	σ	h (mm) (h/δ)	$\Delta X_{Vc}/c$ ($\Delta z/c$)	Cavitation regime	Comments
Xu <i>et al.</i> ¹⁸⁰ (2020)	A cavitator on the lower side of the NACA0012 foil ($c = 38.1$ mm, $S = 152.4$)	NA	1–12	0.1, 0.2, 0.04	5 mm	3.125%, 6.25%, 12.5%, 25%	Super-cavitation	Changing the cavitation shape affects the pressure distribution around the hydrofoil limitation to the effectiveness of the cavitator used for enhancing lift coefficients, since the cavity cannot grow continuously at the cavitator to enclose the hydrofoil in the flow.
Chen <i>et al.</i> ¹⁹¹ (2021)	Delta-shaped counter-rotating VGs on Aeronautics 66 hydrofoil at two different positions ($c = 100$ mm, $S = 150$ mm)	1 m/s (1×10^6)	4–12	0.1–5	0.1 mm	0.1% and 0.45%	Cavitation inception	Vortex generators located at the upstream of the laminar separation point promote the earlier inception cavitation and induce the fingerlike vortex cavitation earlier Vortex generators located in the laminar separation zone delay the inception

The flow over the leading edge of a smooth surface is laminar, and at some point, it becomes turbulent as a result of a flow instability. A thin layer of laminar flow forms along the length of a smooth surface after transiting into a turbulent boundary layer [Fig. 10(a)]. Figure 10(b) illustrates how roughness on the surface of a flow can cause flow instability upstream, resulting in increased turbulence disrupting the viscous layer, causing the roughness layer to form, affecting pressure drop and heat transfer.⁷² Therefore, boundary layer separation and cavitation can be controlled by transitioning to turbulent boundary layers earlier and increasing momentum near the surface.

The first studies, which considered leading-edge roughness to investigate its effect on boundary layer separation, was conducted by Dryden⁷³ and Kerho and Bragg.⁷⁴ The authors observed that the roughness induced boundary layer transition from laminar to turbulent flow has a completely different mechanism than a natural transition in the smooth airfoil and, the roughness moved trigger of transition to, or very close, the trailing edge of the roughness. Stutz⁷⁵ investigated the influences of the roughness and divergent geometries located beneath the internal two-phase flow's cavity. The study concluded that the roughness could not significantly affect the void fraction distribution, cavity area, and time-averaged velocity. Other findings included that cavity roughness does not impact skin friction drag.

Coutier-Delgosha *et al.*⁷⁶ focused on the wall roughness and its effect on the unsteady behavior of the cavity flow. They observed a significant rise in the frequency of oscillations and a decline in the intensity of pressure fluctuations. A significant reduction in the cavity length was also observed. A study by Ausoni *et al.*^{77,78} examined the effects of tripping the turbulent boundary layer on the wakes of blunt trailing edge symmetric hydrofoils under one specific condition. The leading-edge transition was shown to promote a more organized vortex shedding with decreased vortex shedding frequencies. In Fig. 9, a top view visualization and measurements of vortex-induced vibrations are shown. As well as confirming the tripped transition, the study also revealed a significant increase in vortex-induced hydrofoil vibration and wake velocity fluctuations. The spanwise organization of vortices was strengthened, as was the strength of the vortices. This reduction in spanwise non-uniformities over the boundary layer was linked to the boundary layer turbulent transition at the leading-edge of the hydrofoil. The study also showed how the roughness induced transition led to the generation of small bubble clouds with potentially detrimental erosive properties (Fig. 11).

The application of 15 μ m sandpaper roughness on the NACA 66 hydrofoil decreased the characteristic lift and momentum coefficients and increased the drag coefficient.⁷⁹ Petkovšek *et al.*⁸⁰ investigated hydrodynamic cavitation behavior from laser-textured surfaces and found major effects on the characteristics of cavitation with sensitivity to type of micro-structuring. By comparison against highly polished cases, the extent of cavitation was reduced with some of the laser-textures.

Emelyanenko *et al.*⁸¹ implemented a superhydrophobic coating on stainless steel operating under cavitation in heavily loaded hydraulic systems. Micro- and nano-textures were developed by a nanosecond infrared laser and studied under long-term continuous contact with water. The hydrophobic properties and chemical stability were confirmed. Additional tests under prolonged exposure to abrasive

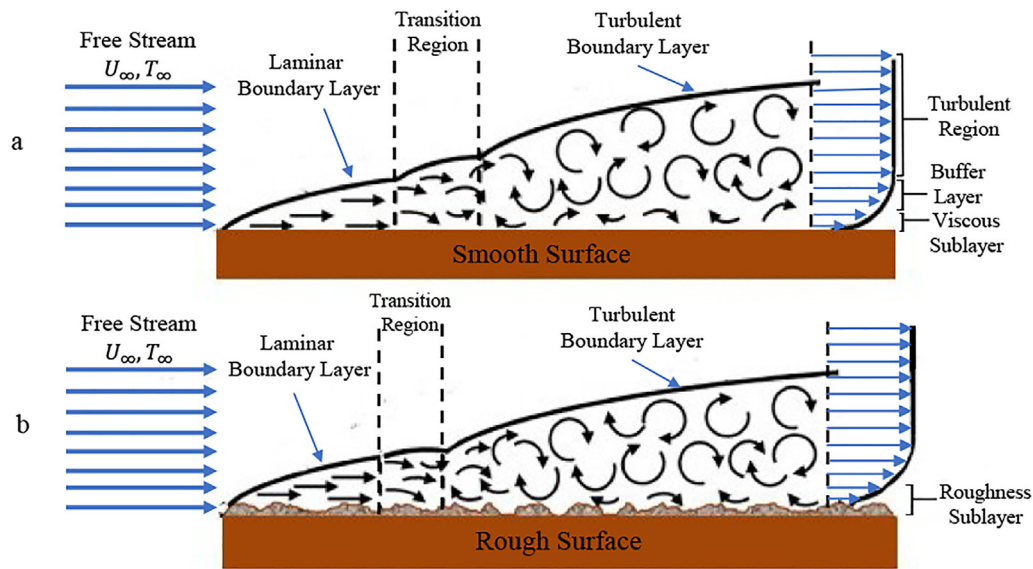


FIG. 10. Boundary layer behavior over (a) smooth surface and generating a viscous sub-layer (b) rough surface where transition to turbulent boundary layer flow happens over a shorter distance from the leading edge and with an increase in instabilities and momentum transfer compared to a smooth surface.⁷²

wear and cavitation loads showed significant improvement to the functional durability.

Cavitation inception and development was investigated using hydrofoils with smooth and rough ($0.4\ \mu\text{m}$) leading edges by Tao *et al.*⁸² According to their research, cavitation inception was enhanced by roughness when incidence angles are below 2° . The roughness element decreases wettability and traps more gas, which can enhance surface nucleation and increase the risk of cavitation. In their studies of hydrofoils with high incidence angles ($>3^\circ$), roughness significantly delayed cavitation incipience while developed cavitation was almost the same between smooth and rough hydrofoils. Based on their argument, this unexpected incipient delay was caused by the boundary layer structure changes due to roughness.

Churkin *et al.*⁸³ also conducted a study to determine how wall roughness impacts the cavitation structure. Under specific conditions, it has been demonstrated that varying the surface roughness type and characteristics can control the formation of cavities. Onishi *et al.*⁸⁴ studied the effects of hydrophilic and hydrophobic coatings on cavitation of tidal turbines and also observed that hydrophilic coating could reduce the incipient cavitation number. A lower growth of cavitation was linked to the hydrophilic of textures, especially at small angles of attack. Issues related to the coating lifetime with loss of effectiveness after 210 s of exposure to cavitation were reported. Hao *et al.*⁸⁵ also used high speed PIV to analyze the cavitation mechanism after the addition of surface roughness over the hydrofoil's entire surface. The results show that the cloud cavitation mechanism changes significantly compared to smooth hydrofoil surfaces. Over a rough hydrofoil, cloud cavitation appears as attached subulate cavities while cavitation over smooth surfaces form finger-structured cavities. The roughen hydrofoil also experienced a longer cloud cavitation period and higher cavitation growth rate.

Chen *et al.*⁷⁰ focused on the effects of localized roughness modification concentrating on the hydrofoil leading edge. They observed that both lift and drag coefficients were increased by surface roughening. The lift-to-drag ratio was also slightly increased, and the incipient cavitation number could be reduced by generating higher turbulent kinetic energy and lowering the minimum surface pressure at the leading edge. The roughness did not affect, however, the formation and transition to cloud cavitation. The change in cavitation patterns in this study is shown in Fig. 12.

The efficacy of a range of artificial roughness types on propeller tip vortex cavitation was also investigated by Asnaghi *et al.*⁸⁶ Both of their numerical and experimental analysis showed that in the case of optimum roughness, tip vortex cavitation inception decreased around 33%, while drag force increased less than 2% compared to the smooth hydrofoil. It is found that compared to the smooth foil, the roughness separation line induces more distribution of vorticity over the tip, which led to the vortex strength reduction.

Svennberg *et al.*⁸⁷ tested two configurations of uniform and non-uniform roughness patterns of $230\ \mu\text{m}$ height applied over an elliptical foil. The roughness has been shown to result in lower angular momentum one chord length downstream of the tip without notable change in the radius of the vortex core. The study found that the cavitation number for tip vortex cavitation inception can be reduced by 33% for a 2% increase in drag by optimizing the roughness pattern. No obvious differences were noted when comparing the effect of uniform and non-uniform roughness distributions on cavitation inception properties. Non-uniform roughness distributions did, however, have a detrimental effect on drag. Also, while the application of surface roughness did not increase the risk of the foil sheet cavity, it was found to impact on the small scale nuclei production. This was explained by the hydrophobic nature of the roughened surfaces, as roughness elements create

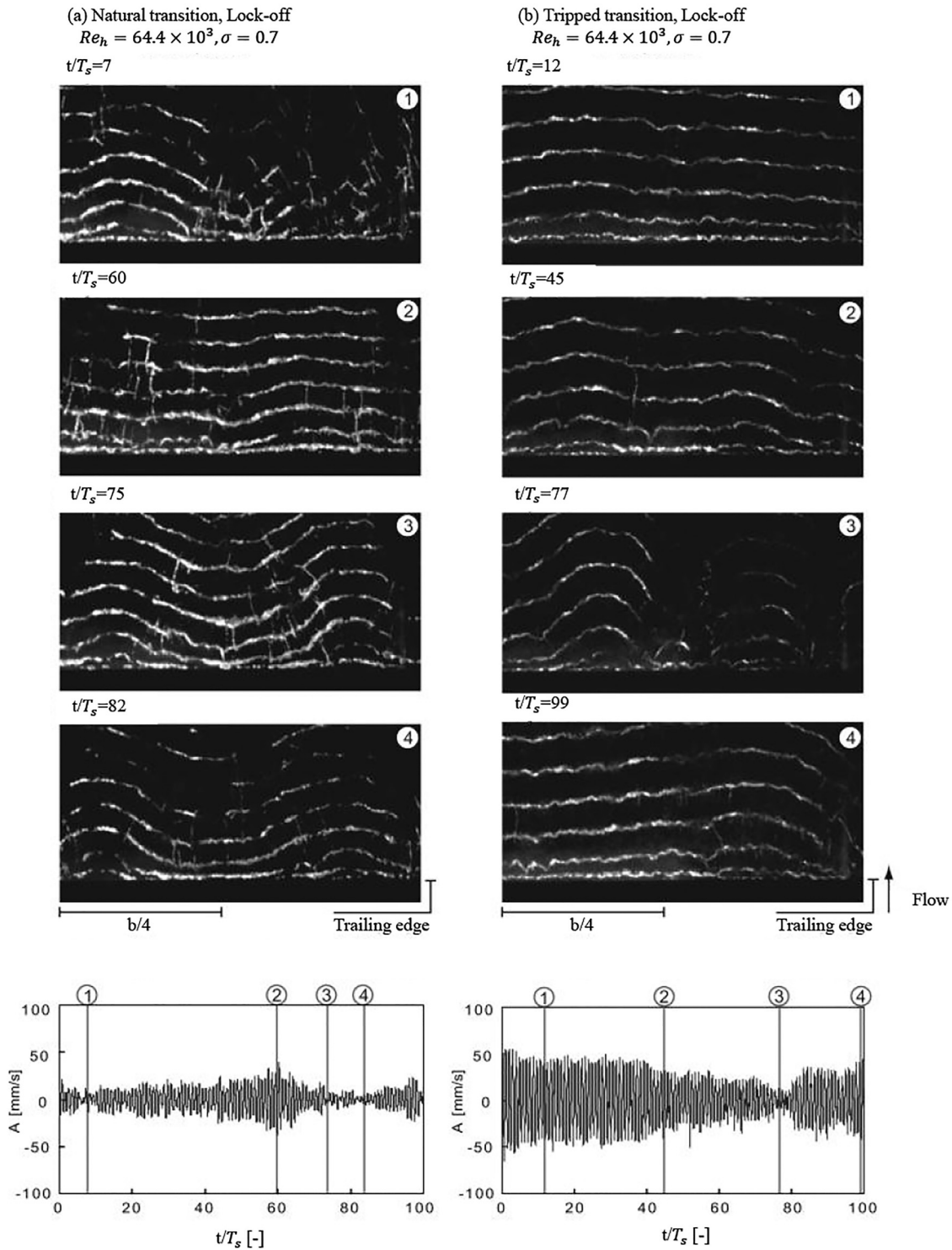


FIG. 11. Cavitation vortex street and vortex-induced vibration signal on the hydrofoil at $Re = 64.4 \times 10^3$ and $\sigma = 0.7$. (a) Natural transition (smooth surface) and (b) tripped transition (with roughness). A direct relationship existed between spanwise vortices and vortex-induced vibration level, and with the rough surface, the spanwise vortices considerably increase intensity and promote a re-establishment of organized vortex shedding.⁷⁸ Republished with permission of Ausoni *et al.*, *J. Fluids Eng.* **134**, 051207 (2012). Copyright 2012 Clearance Center, Inc.

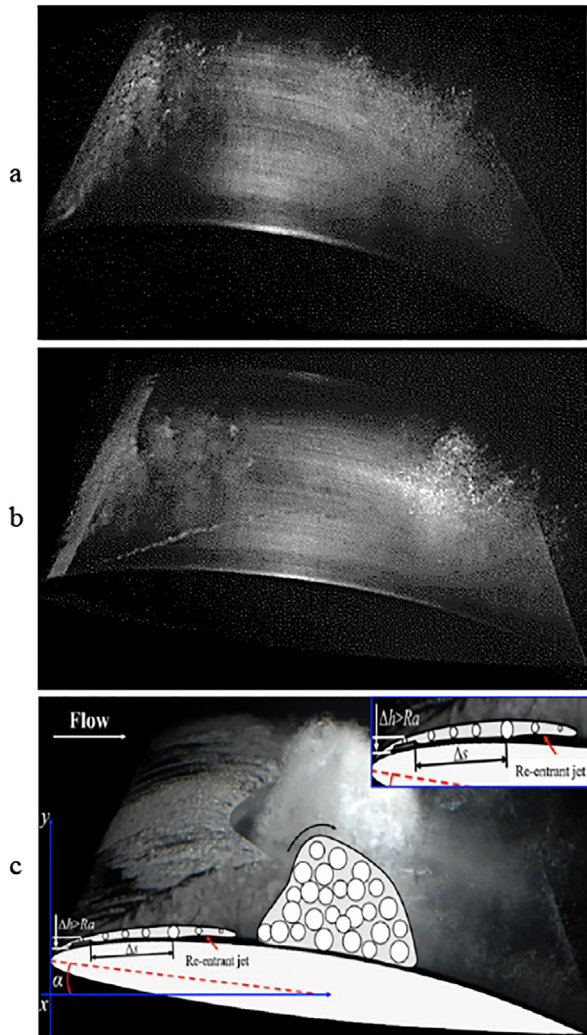


FIG. 12. Cavitation patterns over a hydrofoil (a) without leading-edge roughness, with $Re = 0.8 \times 10^6$, $\sigma = 2.5$, and $\alpha = 8$, and observation of sheet cavitation, (b) with leading-edge roughness, with $Re = 0.8 \times 10^6$, $\sigma = 2.5$, and $\alpha = 8$, showing incipient cavitation and (c) with leading-edge roughness at $Re = 1.0 \times 10^6$, showing the formation of cloud cavitation. High-pressure gradients initiated the formation of re-entrant jets toward the leading edge of the cavity during the initial stage. Thereafter, the cloud cavity characterized by a high vapor fraction rises away from the surface when the height of the cavity (Δh) is greater than the roughness (Ra). Furthermore, there is enough distance between the leading edge roughness and the re-entrant jets (Δs), and therefore, the local pressure distribution on a leading edge is greatly affected by the leading edge roughness.⁷⁰ Reprinted by permission from Chen *et al.*, *Acta Mech. Sin.* **36**, 1202 (2020). Copyright 2020 Springer Nature Customer Service Center GmbH: Springer Nature.

nano- and micro-sized residual air pockets from which small nuclei are continuously produced as a result of local degassing.

The study of cavitation extends beyond inception, and a significant research effort has been dedicated to the study following growth and collapse stages of cavitation. Published studies^{88–90} have considered the effect of shock waves,^{91–94} refraction wave^{91,95–100} thermal

growth^{95,101–109} and fluids properties,^{107,110,111} and, in particular, liquid compressibility and viscosity^{110,112–117} and the presence of non-condensable gas.^{118–120} Not many studies, however, have focused on the effect of passive flow control on bubble growth and collapse. The most likely reason for this is the clearer role played by surface modification in controlling boundary layer separation than bubble growth and collapse. One notable exception is the work by Kadivar *et al.*¹²¹ who recently used a rigid aluminum plate with shark skin-inspired micro-structured riblets to investigate the effects of regular surface roughness on the bubble dynamics of a single cavitation bubble. A micro-structured V-shaped riblet was used to study the dynamics of a single laser-generated cavitation bubble. During the first collapse, microbubbles formed between the bubble and the riblet surface were shown to reduce the momentum of the micro-jet produced by the collapse. The micro-structured riblets were then linked to a reduction in extent of cavitation-induced erosion. A recent study by Gonzalez-Avila *et al.*¹²² also proposed a biomimetic gas entrapment by micro-textured surfaces (GEMS) derived from the mushroom-shaped features found in hairs and cuticles of sea skaters and springtails. The GEMS, produced by using SiO_2/Si substrates and micro-fabrication techniques, were shown to trap air when immersed in water. The entrapped air, in turn, was shown to repel cavitation bubbles and protect against cavitation erosion. The process of formation, growth, and collapse of cavitation bubbles is illustrated in Fig. 13 with and without surface topographies. Experimental results presented demonstrated the effectiveness of the technique for a wide range of bubbles to surface distances.

A summary of important studies for cavitation control using surface roughness is presented in Table III.

B. Blade profile and geometry modification

Direct optimization of the blade profiles and geometries can also contribute to cavitation mitigation. Some of the earliest studies in this respect relate to efforts dedicated to the development of a series of nonsymmetrical hydrofoils specifically designed to reduce the cavitation bucket in practical applications. Cavitation bucket is a diagram which can characterize the cavitation inception by presenting how minimum pressure coefficient (C_{pmin}) vary with angle of attack (Fig. 14). Results indicate that a significant delay in cavitation inception could be achieved.^{123,124}

Kyparissis and Margaris^{125,126} worked on different centrifugal pump blade designs, including double-arc synthetic blades and different blade leading edge angles. The investigation considered pump hydraulic performance and cavitation in tandem. The blade leading-edge angles were experimentally tested over a range of 9° , 15° , and 21° . For low and high angle, attached cavitation was found to move from the pressure to the suction side, respectively, while cavitation could be eliminated 15° blade leading edge angle of attack. It is because the testing condition is close to that of the best efficiency point. Increasing the blade leading angle of attack in this study could increase the total head and efficiency. Other studies have documented the benefit of increasing the blade leading edge. Shi *et al.*¹²⁷ applied a biomimetic tubercle on the design of a tidal turbine leading-edge. They observed that the appendages could constrain the extent of the cavitation region but this was achieved at the cost of higher cavitation number and earlier onset of cavitation.

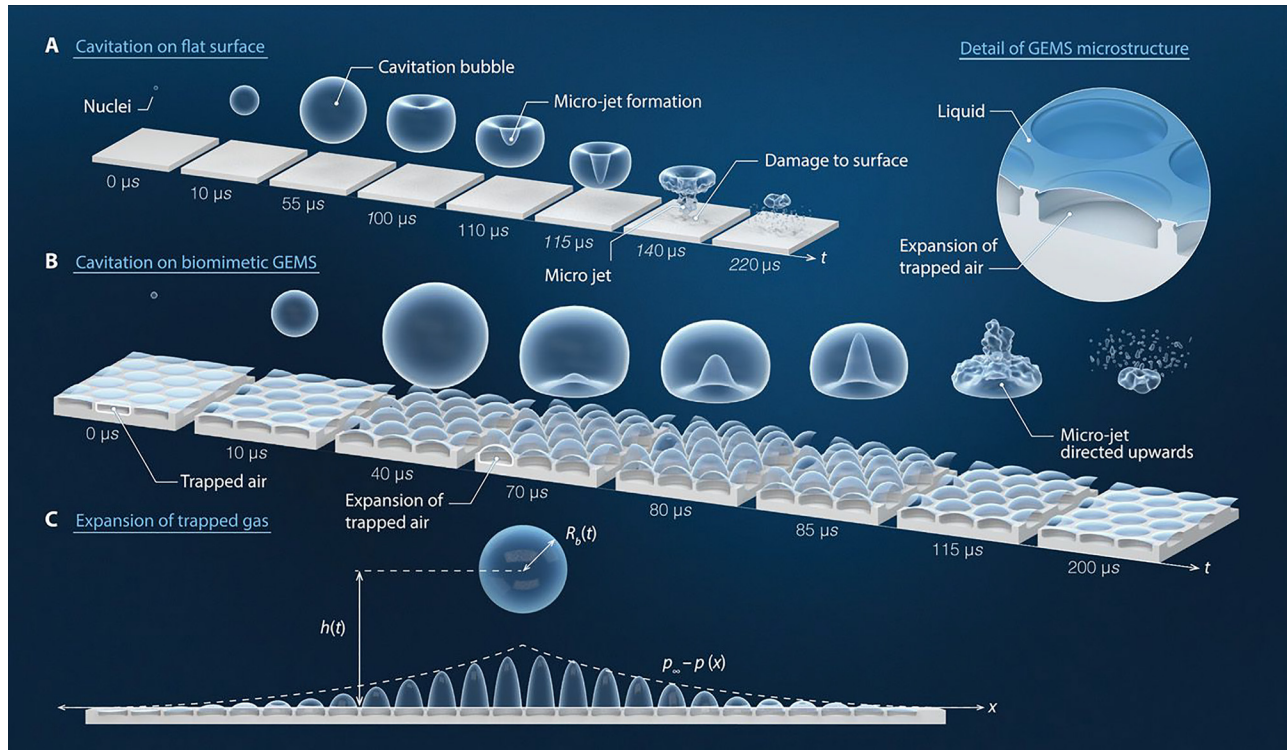


FIG. 13. Gas entrapment by micro-textured surfaces as a means to prevent cavitation damage showing illustrations of (a) the cavitation process over a flat surface with a micro-jet generated from a bubble collapsing above the substrate surface, which is a key factor in cavitation induced erosion, (b) the cavitation process on biomimetic gas entrapment micro-textured surfaces, showing the entrapped gas deflecting the liquid jet's direction upward thereby protecting the surface substrate from the cavitation bubble pressure jet, and (c) the expansion of entrapped gas as a result of nearby cavitation bubble pressure field.¹²² Reproduced with permission from Nguyen *et al.*, *Sci. Adv.* **6**, eaax6192 (2020). Copyright 2020 Authors, licensed under a Creative Commons Attribution (CC BY) license.

As the shape of the blade tips can have a significant effect on tip leakage, foils with various tip shapes, such as squealer tips,^{128–130} thickened tips,¹³¹ rounded tips,^{132,133} and C-grooves¹³⁴ have been studied. The casing grooves may also serve as an effective solution for suppressing the tip-leakage vortex (TLV), according to Kang *et al.*¹³⁵ and Hah *et al.*¹³⁶ It has been confirmed, however, that the effect of passive control strategies in the control of tip leakage is greatly influenced by gap size.¹³⁷

The study by Custodio *et al.*¹³⁸ focused on the characteristics of cavitation inception with wavy leading-edge patterns. The authors found that hydrofoils with medium and large protuberances can confine the cavitation region behind the protuberance troughs. By contrast, standard hydrofoils showed sheet cavitation over the entire span. Zhao and Wang¹³⁹ conducted numerical simulation to determine the effect of the bionic fin-fin structure on cavitation on a hydrofoil surface. Their results showed that these structures are able to increase the lift-to-drag ratio and decrease the turbulent kinetic energy and would be an effective passive control method for cavitation. A novel design for a hydrofoil with twin protuberances to mimic the two prominent tubercles found on the flipper of a humpback whale was proposed and studied by Kant and Bhattacharyya.¹⁴⁰ This design was characterized by its ability to limit the separation zone between the chordwise vortices shed from the two humps at high angles of attack ($>20^\circ$).

Although the pre-stall lift coefficient achieved by the modified profile was lower, the maximum lift was increased. The two protuberances were found to reduce the extent of stall separation by altering the interaction of the two chordwise vortices over the suction side, resulting in an enhanced lift after stall. At pre-stall and post-stall angles of attack, the amplitude and spacing of the two protuberances had an important impact on the lifting characteristics. It has been determined that such modifications can effectively control flow at high angles of attack and can be tailored for specific marine applications.

The leading-edge protuberances of humpback whale flippers were also incorporated in hydrofoil modifications by Li *et al.*¹⁴¹ to study the impact on cavitation. The wavy leading edge considered improved the lift–drag characteristics and reduced cavitation volume by around 30%. The shedding of cavitation bubbles was also stabilized by reducing the wavelength and increasing the amplitude of the shape modification. Increasing the amplitude significantly reduced the cavitation volume, decreased the amplitude of pressure, and overall enhanced the suppression of cavitation.

According to a recent study of a hydrofoil with flipper protuberances on the leading edge,¹⁴² the hydrodynamic performance and cavitation characteristics were significantly affected. A flow visualization illustrates how the hydrodynamics and pressure distributions of modified hydrofoils result from periodic and symmetric streamwise vortices

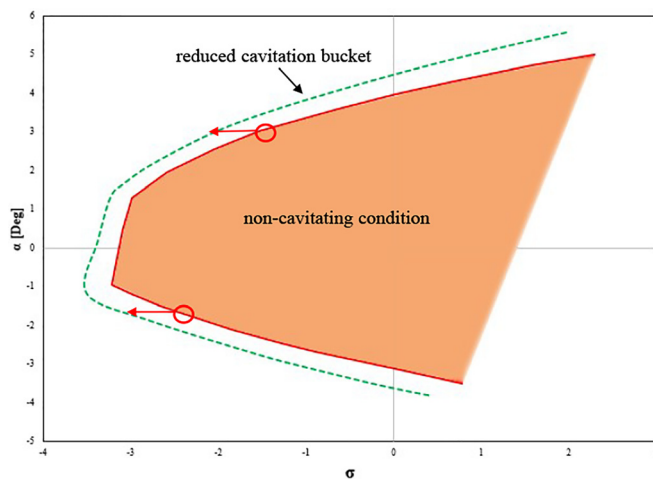


FIG. 14. The cavitation bucket diagram can predict the cavitation inception based on the cavitation number or minimum pressure coefficient and angle of attack in a specific pump. Reducing or moving the cavitation bucket to a lower cavitation number can be a target as it shows a delay in cavitation inception.

that originate from protuberances. The location and scale of cavitation are considerably restricted by the streamwise vortices of modified hydrofoils. The relationship between pressure fluctuations and cavity evolution is also analyzed with a simplified one-dimensional model. Their results showed cavity volume acceleration is attributed to pressure fluctuations, which can be used to control cavitation oscillations in engineering designs.

C. Grooves

Grooves and riblets are defined as streamwise channels on the surfaces and have been extensively studied for their drag reduction properties.^{143–145} They have also shown potential benefits for cavitation control. A numerical and experimental study was undertaken by Li *et al.*¹⁴⁶ to examine how distributed grooves affected cavitation around the body of revolution. Numerical simulations showed that the grooves accentuated the pressure variations along the tunnel. Grooves also resulted in significant fluctuations of pressure on the surface. According to both experimental and numerical results, groove width was shown to affect the amplitude and interval of fluctuation and, therefore, the cavitation distribution.

Following a study on the benefit of surface roughness on unsteady shedding of cloud cavitation, Danlos *et al.*¹⁴⁷ investigated longitudinal grooves and their effect on sheet cavitation. Grooves were found to suppress cloud cavitation instabilities.¹⁴⁸ Liu and Tan^{134,149} studied grooves' effects on suppressing tip vortices, which are precursor to cavitation inception. The analysis confirmed the ability of grooves to suppress the leakage vortices near the leading-edge of the hydrofoil subject to careful positioning.

To control TLV cavitation, overhanging grooves (OHG) were fitted to hydrofoils by Cheng *et al.*¹⁵⁰ A significant improvement in cavitation suppression was observed with the OHG compared to the baseline, conventional grooves and anti-cavitation lip (ACL) with a minimal effect on hydrofoil performance. Effective reduction in the

intensity of TLVs and tip-separation vortices was achieved with small gap sizes. The OHGs were shown to increase the TLV core size when the gap size was in the medium to large range, increasing, in turn, the minimum local pressure. OHGs were also examined for their effect on hydrofoils, indicating that they can effectively suppress the fluctuation of TLV cavitation without significantly altering the time-averaged drag or lift.

D. Drainage and injection

Another important family of passive flow control methods relies on drainage and injection. Kato *et al.*¹⁵¹ developed a method based on the water discharge from a slit from the hemispherical shaped leading edge. The momentum injection created a wavy motion in the boundary layer with a wavelength higher than the boundary layer thickness. This transitional flow motion could generate an inflection in the velocity profile and disturb the separation zone. It was shown that sheet cavitation on the hydrofoil could be suppressed completely. Arndt *et al.*¹⁵² also found that the injection of air on the leading edge of a NACA 0015 hydrofoil minimized cavitation erosion.

The application of bleed and jet reinjection flow control on turbopumps were investigated by Japikse.¹⁵³ The auto-oscillation region on the pump impeller suction surface was eliminated, and cavitation happened at a lower cavitation number, while also improving the pump's total head and efficiency, and increasing the suction's specific speed.

Zhu *et al.* and Bing and Hongxun^{154,155} studied gap drainage in the centrifugal pump impeller as illustrated in Figs. 15(a) and 15(b). The approach was shown to act on cavitation while improving the pump hydraulic performance. A new type of cavitation was observed due to a change in the discharge flow due to drainage and the cavitation volume in the impeller channel.

The effect of water injection on cavitation suppression over NACA0066 hydrofoil was also investigated by Wang *et al.*¹⁵⁷ An optimization of the position and angle of the jet were shown to have a significant effect on cavitation suppression. According to this study, this type of water injection can increase the boundary layer's velocity gradient and decrease the extent of flow separation. A decrease in the thickness of the recirculation zone and, consequently, of the re-entrant jets' velocity were also observed.

Kamikura *et al.*¹⁵⁶ implemented an asymmetric slit on the axial inducer's blades to observe specifically to study the effect on cavitation, as shown in Fig. 14(c). Results showed that this technique is effective on cavitation instabilities suppression while they were installed in the proper arrangement. It was observed that by viewing the flow field in a circumferential direction around the slit near the blade tip, the wave from the jet divided the cavity, which then decreased the cavity volume. Furthermore, the asymmetric arrangement of the slit in the inducer can disturb the regularity of rotating cavitation because the slit flow rates differ differently in each blade. The summary of important studies in the blade profile and geometry modification, drainage and injection, and grooves and slits is presented in Table IV.

E. Obstacles

Early investigations of the effect of flow obstacles were precursors to VG studies. Kawanami *et al.*¹⁵⁸ studied the structure of cloud cavitation in the wake of obstacles on hydrofoils. As re-entrant jets were

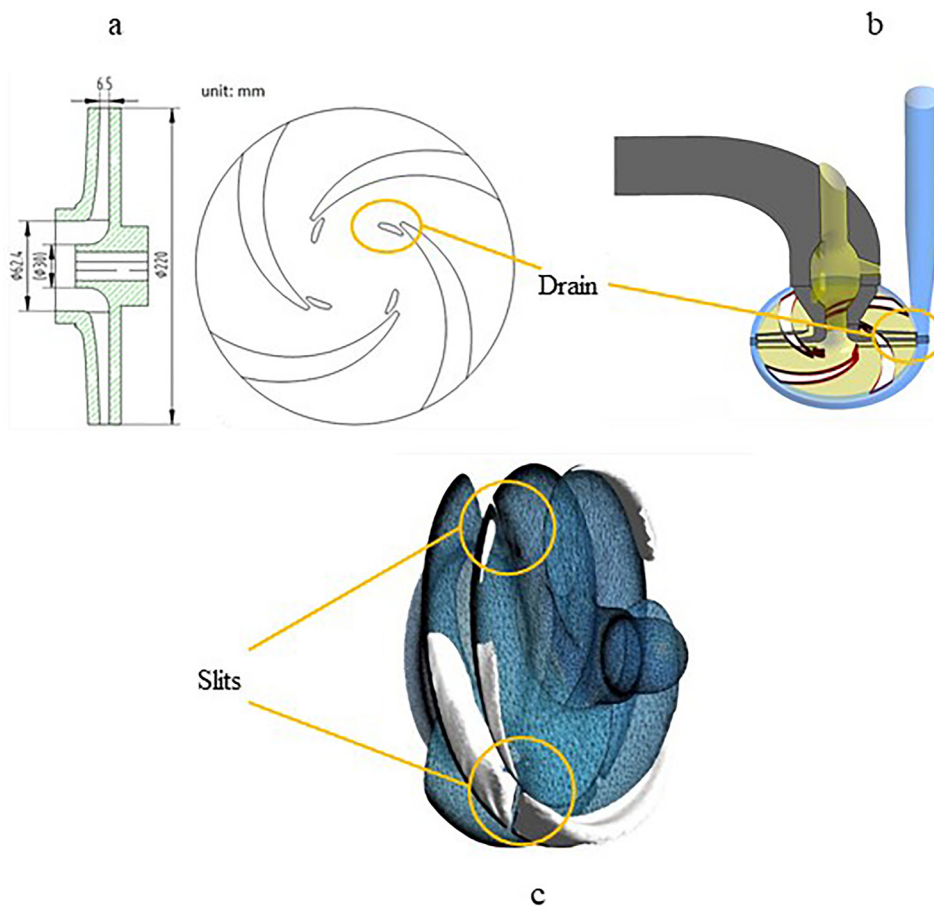


FIG. 15. (a) and (b) Schematic of the gap drainage impeller in the physical pump and computational region.¹⁵⁵ Republished with permission from Z. Bing and C. Hongxun, *J. Fluids Eng.* **139**, 031301 (2016). Copyright 2016 Clearance Center, Inc. (c) Modeling of the inducer with the slit under the cavitation condition.¹⁵⁶ Republished with permission from Kamikura *et al.*, *IOP Conf. Ser.* **240**, 032044 (2019). Copyright 2019 Authors, licensed under a Creative Commons Attribution (CC BY) license.

shown to affect the periodic shedding and generation of cloud cavitation, the obstacle on the foil was able to block the re-entrant jet off, consequently preventing the generation of cloud cavitation. In comparison with hydrofoil without obstacle, the noise intensity and hydrofoil drag were remarkably reduced. After this seminal work, several studies have continued to explore the interaction between obstacles and cavitation instabilities.^{159–162} Enomoto *et al.*¹⁶³ presented a study in which obstacle plates were attached upstream of helical inducers in order to suppress cavitation surges observed under partial flow conditions. Installing axi-symmetric and axi-asymmetric obstacle plates of ring type could narrow the range of the onset regions of oscillating cavitation surge. Obstacle plates with a blockage factor of 30% reduced cavitation surge oscillations to a negligible level. The suppression effects became greater with the increased blockage factor. In a follow up study on inducer performance and cavitation surge suppression, Kim *et al.*¹⁶⁴ considered two kinds of inducers with blade tips of 8° and 14° . The experimental study considered various axial positions of the obstacle to inducer inlet and various blockage ratios against the flow passage area. A blockage of about 50% between the flow passage and the obstruction was recommended as the optimal ratio. The most appropriate axial position of the obstacle upstream of the inducer inlet must take account of the inducer blade angle with a smaller blade angle requiring a shorter distance. Axis-asymmetrical obstacles were

also shown to cause vibrations even under normal operating conditions at high Net Positive Suction Head (NPSH).

Huang *et al.*¹⁶⁵ used a trip bar on an axisymmetric projectile to weaken the re-entrant jets and pressure wave propagating from the collapse of cavities. An investigation of supercavitating flow was conducted around three different conical cavitators with wedge angles of 30° , 45° , and 60° by Kadivar *et al.*¹⁶⁶ The wedge angle of the cavitator was found to be the most effective design criteria to increase the cavity length. The results have shown that as cavitation number decreases, drag coefficient decreases, and the drag coefficient of a cavitator increases with the increasing wedge angle when inlet velocity is constant. The cavity length was increased both for the lower and higher supercavitation conditions studied numerically. Che *et al.*¹⁶⁷ focused on a spanwise obstacle located on the suction side of the hydrofoil shown in Fig. 16. The near-wall pressure increased in the wake of obstacles and led to suppression of sheet cavitation. The hydrofoil modification, however, had little impact under transitional cavity oscillation most likely because of the inherently unstable flow as shown in Fig. 17.

Positioning the obstacle downstream of a flat hydrofoil was investigated by Zhang *et al.*¹⁶⁸ While no significant change in the average cavity length was observed at equivalent cavitation number, the obstacle did affect the dynamics, strength and direction of re-entrant jets.

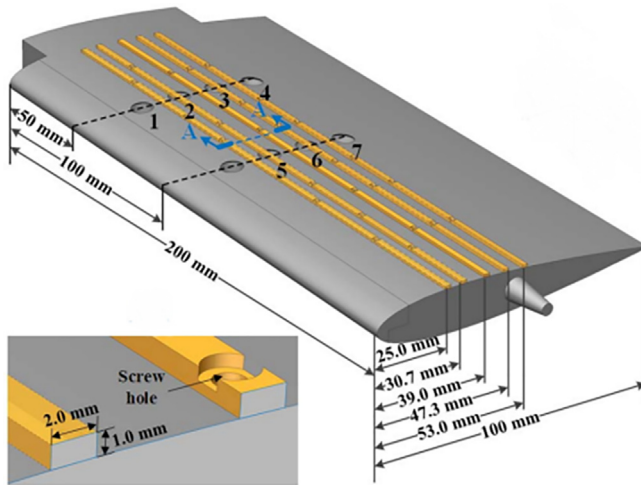


FIG. 16. Representation of spanwise obstacles on NACA0015 hydrofoil at different positions.¹⁶⁷ Reprinted by permission from Che *et al.*, *J. Mech. Sci. Technol.* **33**, 4265 (2019). Copyright 2019 Springer Nature Customer Service Center GmbH, Springer Nature.

Using obstacles for control of baled cavitation in water jet pumps is investigated by Zhao *et al.*¹⁶⁹ They implemented a pair of tandem obstacles on the suction side of the pump. It is observed that there is more resistance against the incipient and the development of

leading-edge cavities after using obstacles. Although shear energetic cavitation appears after obstacles with foamy wakes, pressure gradients analysis shows that these obstacles were effective in blade cavitation. However, the hydraulic performance loss, including 6% head drop and 5.6% efficiency drop, was observed because of violent pressure fluctuations after using obstacles on the blade.

A recent study by Lin *et al.*¹⁷⁰ has analyzed the influence of arc obstacles on the evolution of cavitation over flat hydrofoils. Experimental evidence has shown that the shedding of cavitation and the distribution of air over the flat hydrofoils are influenced by the obstacles. The arc obstacles were shown to stabilize the leading edge of the shedding cavity and restrict its size, which inhibits cavitation.

F. Vortex and bubble generator

The ability of VGs to control boundary layer separation has been exploited on hydrofoils to destabilize attached cavities. The schematic of Fig. 18 (Ref. 171) illustrates how counter-rotating vortices generated upstream of the cavity by the VG delays separation and promotes the formation of a smaller cavity with a growth and shedding behavior similar to the attached cavity generated by laminar boundary layer separation but with some important distinction. Its leading edge is observed to move dynamically, likely due to a thin liquid layer separating the cavity from the wall as conjectured by the authors, and the cavity edge shows oscillations indicative of a turbulent flow.

The low-pressure core of the streamwise vortices induces stable vortex cavitation, which breaks down into bubble clouds upstream of the attached cavity. Similar observations were made in a study of VGs

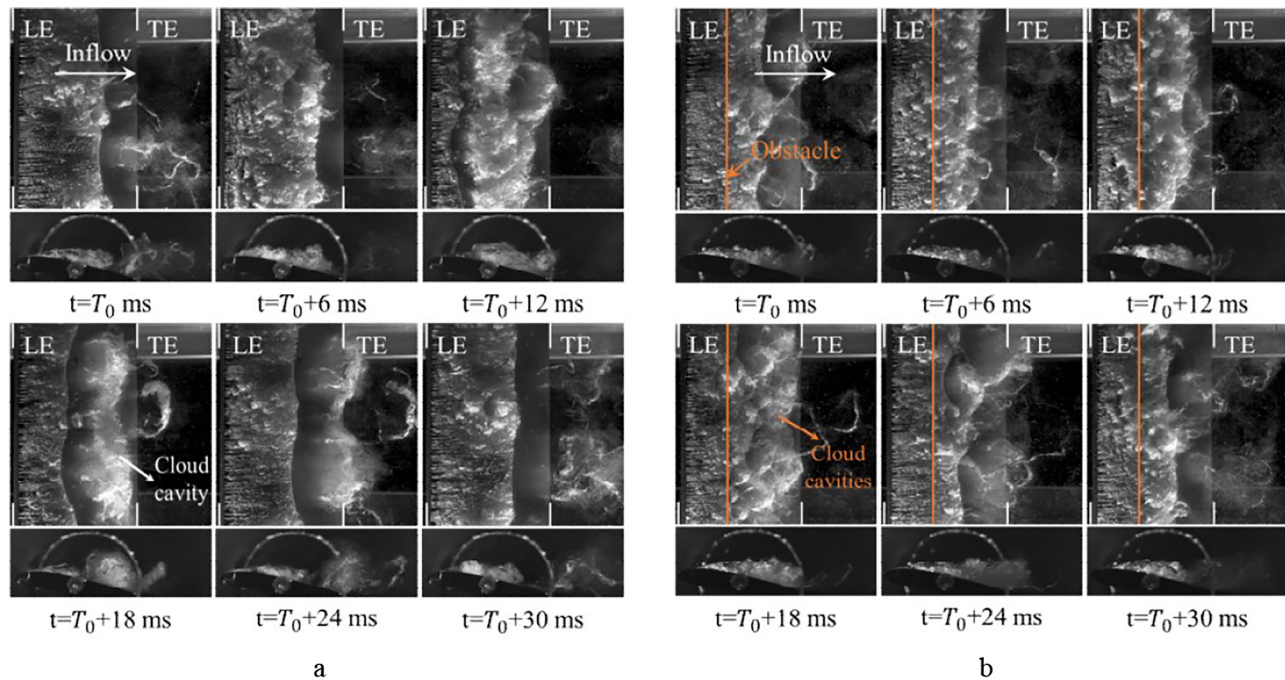


FIG. 17. (a) A typical partial cavity oscillation period on a smooth hydrofoil involves the development of sheet cavitation, the propagation of re-entrant jets, and the shedding and collapse of cloud cavities, (b) a hydrofoil with an obstacle under the same condition. The obstacle inhibits re-entrant jets during partial cavity oscillations, thereby suppressing cloud cavitation. As a result, the cavity fragments, and the cloud cavitation collapses to a non-uniform small-scale cloud.¹⁶⁷ Reprinted by permission from Che *et al.*, *J. Mech. Sci. Technol.* **33**, 4265 (2019). Copyright 2019 Springer Nature Customer Service Center GmbH, Springer Nature.

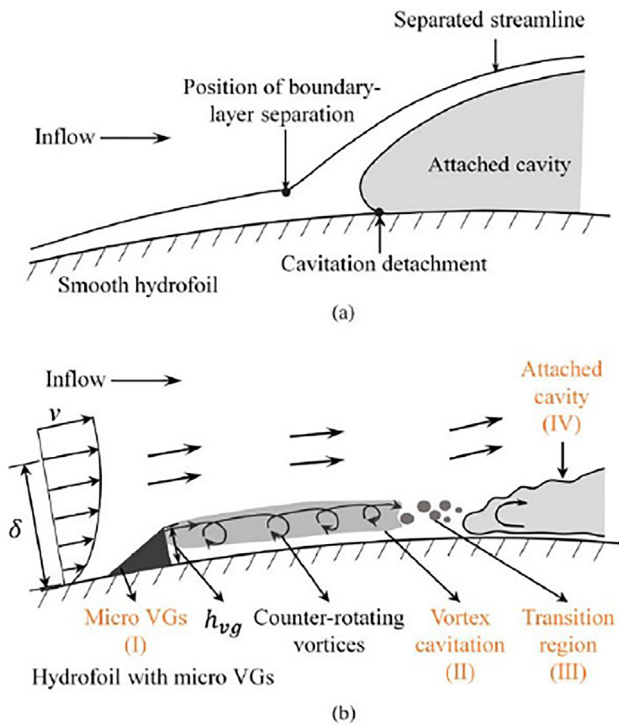


FIG. 18. Schematic description of attached cavitation over (a) a smooth hydrofoil; a typical process of attached cavitation formation and (b) a hydrofoil with micro-vortex generators where (I) and (II) every standalone micro-vortex generators induces counter-rotating vortices at the end of their trailing edge and develop micro-vortex cavitation, (III) a narrow transition region exists between vortex cavitation and attached cavitation, which is caused by shedding several small bubbles produced by vortex cavitation, and then in (IV), attached cavitation is developed without glossy and divot structures observed in smooth hydrofoil.¹⁷¹ Reprinted with the permission from Che *et al.*, *Phys. Fluids* **31**, 044102 (2019). Copyright 2019 AIP Publishing.

by An.¹⁷² The application of VGs in control of cavitation in multipulsion vessels was studied by Liang-mei.¹⁷³ They found a significant improvement in cavitation instability and declining pressure fluctuation.

The application of bubble generators on cavitation control was studied by Javadi *et al.*¹⁷⁴ through a two-dimensional cavitation calculation. This bubble generator was actually a wedge type VG. Their numerical analysis showed that this VG can make a low pressure recirculation region (below saturation pressure) behind the VG. Bubbles then start to generate and grow in this region. By controlling this condition, the bubbly flow becomes stable and will not vanish, or in other words, interfere and stop the cavitation process. They observed that the whole cavitation process, including vaporization, bubble generation, and bubble implosion, could be affected, and lift and drag fluctuations could be reduced.

Vortex generators that have been optimized can also be used for TLV cavitation suppression. The experimental results of Amini *et al.*¹⁷⁵ have shown that the winglets could effectively increase the radius of the tip vortex and delay the initial inception of the TLV cavitation process. The ACL, however, is the only proposed method that

has actually been applied. Results showed that it is difficult for the ACL to have a satisfactory inhibitory effect on TLV cavitation, and once the vortex generators are not operating under design conditions, a more intense level of cavitation will be induced.^{137,176}

A recent numerical study by Kadivar *et al.*¹⁷⁷ proposed a new type of VG called cavitating bubble generators (CGs) (Fig. 19). The CGs were adopted from wedge-type VGs were used before for aerodynamics application with the aim of generating cavitating bubbles at the suction side of hydrofoil. They observed that the high momentum fluid from the free stream flow moved to the hydrofoil's near-wall low energy region. These CGs could generate vortices downstream and move higher kinetic energy flow to the vicinity of the hydrofoil surface. Consequently, quick high-pressure pulsations near the hydrofoil surface were reduced, and the resistance against pressure rise before boundary layer separation was increased. They found that the vortex structures were significantly modified on the suction side and the hydrofoil wake region. This phenomenon suppresses the cyclic behavior of unsteady cloud cavitation and declining turbulent velocity fluctuation in that area. The experimental investigation of CGs proved an essential role of re-entrant jets on cloud cavity shedding structure.¹⁷⁸ Their experiment proved the reduction of pressure pulsation's amplitude in instabilities of cavitation dynamic. As a result, they can be used as a useful tool for delaying cloud cavitation formation. A comparison between hydrofoil with and without CGs is presented in Fig. 20. In another study, a CG was installed adjacent to the cavitation inception on a semi-circular leading-edge flat plate to control and manipulate unsteady dynamics of cavitation surge. The CG was shown to mitigate large-scale cavities, suppress the spanwise instability of adjacent cavities, and suppress large-scale cavities over the flat plate. Passive control was observed to reduce the dominant frequency of pressure pulsations.¹⁷⁹

Xu *et al.*¹⁸⁰ used cavitators placed at various locations on a hydrofoil's bottom surface to study the supercavitation flow around it. As their observations showed, a localized high-pressure region appears between the leading edge of the hydrofoil and the cavitator, and downstream of the cavitator, the pressure is equal to the saturated vapor pressure of water. Based on the magnitude and distribution of pressure on the hydrofoil surfaces, the lift coefficient increased as the cavitator was positioned farther away from the leading edge and toward the

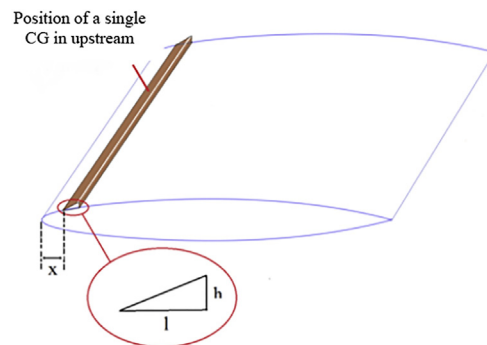


FIG. 19. Analysis of wedge-type cavitating bubble generators located on the suction side of a hydrofoil was found to reduce high-pressure pulsations, alter boundary layer separations, and alter vortex structures.¹⁷⁷ Reprinted with permission from Kadivar *et al.*, *Appl. Math. Model.* **64**, 333–356. Copyright 2018 Elsevier.

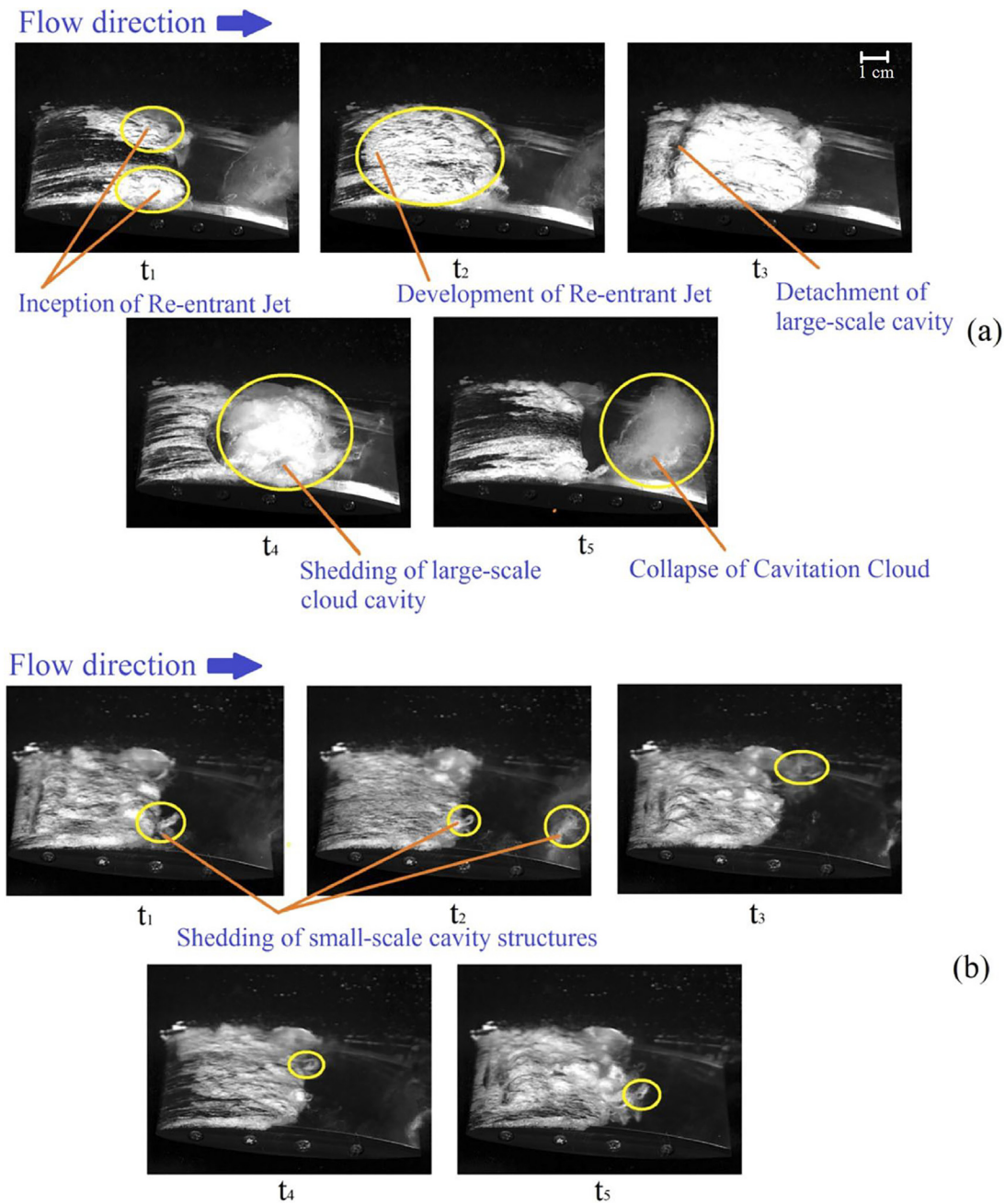


FIG. 20. Structure of cavitation over a hydrofoil with attack angle of 7° , $\sigma = 1.3$, and $Re = 1.4 \times 10^6$. (a) CSmooth hydrofoil: (t_1) and (t_2) formation and development of sheet cavities and jets, (t_3) detachment of large-scale cavities, (t_4) shedding of large-scale cavitation clouds, and (t_5) collapse of cavitation clouds. (b) Hydrofoil with cavitating bubble generators: inception and shedding of small vortex cavitation over hydrofoil and suppressing could cavitation.¹⁷⁸ Reprinted with the permission from Kadivar *et al.*, Phys. Fluids **32**, 052108 (2020). Copyright 2020 AIP Publishing.

trailing edge. Alternatively, there was a strong correlation between drag coefficients and the maximum thickness of cavitating wakes, which was used as a proxy for the drag coefficient.

Kadivar *et al.*¹⁸¹ also examined a single spanwise row of cylindrical obstacles named cylindrical cavitating bubble generators (CCGs),

shown in Fig. 21. Similar effects were observed such as a reduction in the adverse pressure gradient at the end of cavity, weakening of re-entrant jets and turning unsteady cavity structure to a quasi-stable cavity structure. As a result, the instability of cloud cavitation was mitigated and the near-wall high-pressure pulsation dampened. One key

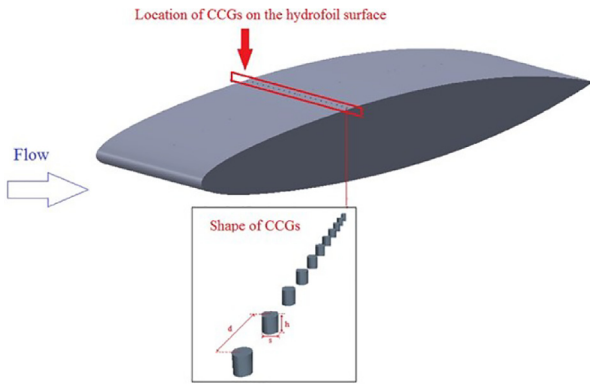


FIG. 21. Hydrofoil with cylindrical cavitating bubble generators located on the suction side where s , h , and d are the diameters, heights, and distances between cylindrical obstacles, respectively. Cylindrical cavitating bubble generators were investigated at locations downstream and upstream of the hydrofoil suction surface. Using the cylindrical cavitating bubble generators, significant reductions were seen in cavitation induced vibration, high wall pressure peaks, and cloud cavitation instability.¹⁸¹ Reprinted with permission from Kadivar *et al.*, *Int. J. Multiphase Flow* **115**, 108–125 (2019). Copyright 2019 Elsevier.

difference to previously studied CCGs is that only small-scale cavity structures are shed while large-scale cavitation clouds are effectively suppressed. It was also observed that vibration-induced cavitation as well as wall-pressure peaks on materials with solid surfaces were significantly reduced.^{181,182} In another study, high-speed visualization, PIV, and a hydroacoustic pressure transducer were used to experimentally analyze the effects of CCGs on turbulence behavior and the amplitude-frequency spectra of pressure pulsations associated with oscillations in the attached cavity length and cloud cavitation instabilities. This study confirmed that CCGs is quite effective at hindering the development of cloud cavitation and at decreasing the strength of middle- and side-entrant jets, which are the primary mechanism that cause unstable cloud cavitation.¹⁸³

Che *et al.*¹⁷¹ considered counter-rotating delta-shaped mVGs built into a quasi-two-dimensional NACA0015 hydrofoil (Fig. 22). The type and geometry of mVG was based on designs from Lin²⁶ and Godard and Stanislas³⁷ reviews to control boundary layer separation using VGs.¹⁸⁴ They designed five counter-rotating delta-shaped mVGs with different h/δ in the range of 0.5–2.5. The ΔX_{VG} were set at 2.5 mm from the hydrofoil leading edge based on the position of boundary layer separation at the leading edge obtained from their 2D numerical modeling results. The study demonstrated that the mVG can suppress the laminar separation under non-cavitating conditions. MVGs located within the viscous sub-layer close to the cavitation detachment point failed to suppress the attached cavitation. Results did show, however, that the transition region and attached cavitation were affected. The authors found that at lower heights relative to the viscous sub-layer, mVGs can generate longer counter-rotating and cavitating vortices within the boundary layer. These mVGs could also fix cavitation inception causing more stable sheet cavitation and cloud cavity shedding. The attached cavitation over the smooth hydrofoil showed a formation of “divot” or “finger” structure as well as two-dimensional Tollmien–Schlichting waves which are shown in Fig. 23. Divots are three-dimensional flow structures which appear near the

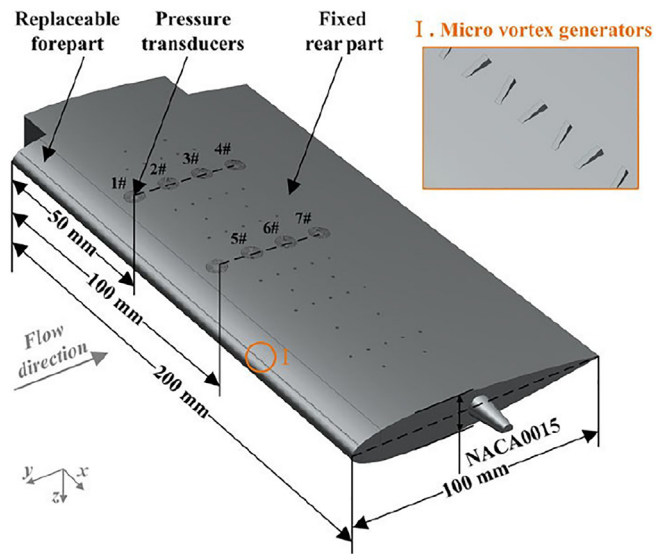


FIG. 22. Schematic of the test hydrofoil with micro-vortex generators. The vortex generators are microscopic delta-shaped counter-rotating vortex generators installed at the leading edge, which were shown to effectively manipulate boundary layer and cavity dynamics in the test.¹⁷¹ Reprinted with the permission from Che *et al.*, *Phys. Fluids* **31**, 044102 (2019). Copyright 2019 AIP Publishing.

cavity interface. They occur at moderately high Reynolds numbers because of local disturbances near cavity interfaces. Upstream of the detachment point, local disturbances were caused by a breakdown of the laminar boundary separation, resulting in a divot when a jet of fluid penetrated the cavity.¹⁹ Tollmien–Schlichting waves are known as streamwise instabilities that occur prior to the transition to

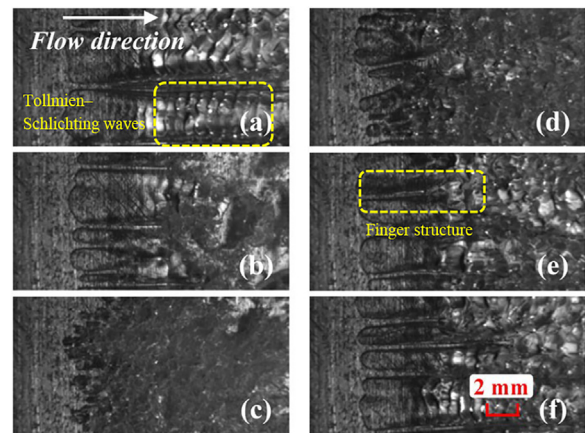


FIG. 23. (a)–(f) Dynamics of cloud cavitation shedding on a smooth hydrofoil. At the leading edge of attached cavitation, typical finger structures are visible. By observing the glossy interfaces of the cavity and the Tollmien–Schlichting waves at the leading edge, laminar separation can be detected. A consistent change in finger structures resulted in cloud cavitation shedding and instability. Cavity collapse occurs when the reentrant jet propagates upstream and reaches the leading edge.¹⁷¹ Reprinted with the permission from Che *et al.*, *Phys. Fluids* **31**, 044102 (2019). Copyright 2019 AIP Publishing.

turbulence in boundary layers. This instability initiates because of the interaction of disturbances with leading edge roughness and can be slowly intensified while moving downstream and can help with the process of turbulence transition.¹⁸⁵ In comparison with a smooth hydrofoil surface, cavitation started closer to the leading edge, eliminating classic “fingering structures” and Tollmien-Schlichting waves.¹⁸⁴

They observed a new structure for cavitation onset while the cavitation onset disappears close to the laminar separation. In the new structure, stable vortex cavitation and subsequent vortex breakdown resulted in bubbly structures, which was finally expressed as an attached cavity region. This vortex break-down was delayed when they reduced the height of mVGs. This delay resulted in a rise in cavitation vortex pattern length. This result showed the potential of mVGs in control of cavity dynamics considering the re-entrant jet penetration depth. The flow visualization of attached cavitation during cloud cavitation without and with VGs in this study is presented in Figs. 23 and Fig. 24.

In another study, Che and coauthors analyzed the instability of the attached cavitation produced with mVGs.¹⁸⁶ This study confirmed that these mVGs are an effective passive control for attached cavitation dynamics and changed the surface wall’s vicinity’s flow dynamics. The results also emphasized again that the mVGs could increase the cavity length and induce counter-rotating streamwise vortices. The mVGs could change the sheet cavity structure to a uniform cavity in a span-wise direction by inducing consistent separate vortex cavitation streaks. The mVGs showed their ability to fix the attached cavitation inception line location, thereby limiting instabilities caused by span-wise disturbances.

In this study, Che *et al.*¹⁸⁶ interpret two types of Rayleigh–Taylor (R–T) and K–H instabilities, while cavity shedding and re-entrant jet interactions happened over a smooth hydrofoil and hydrofoil with mVGs. Re-entrant jets are generated by exposing cavity closure to an adverse pressure gradient. After propagating upstream, these

re-entrant jets impact the cavity interface, causing the cavity to shed. It is possible to interpret the interaction of re-entrant jets and cavities as an R–T. A re-entrant jet and cavity interface at the leading edge interact, generating several cavitating vortices that are indicative of the K–H instability. The K–H instability interpretation has been explained by different shearing velocities causing cavity shedding.

Che *et al.*¹⁸⁶ presented evidence that reverse flow beneath the attached cavities, which were linked to R–T and K–H instabilities, were suppressed. The mVGs were shown to influence partial cavity oscillations, transitional cavity oscillations, and transition between these two instabilities. Experimentation was extended to measure cavitation erosion and analyze impulsive loading from cavity collapse as a measure of the intensity and aggressiveness of cavitation structure with mVGs.¹⁸⁷ The study also included an analysis of the dynamic behavior of the re-entrant jet, shown in Fig. 25. The effect of the mVGs included suppression under certain condition of periodic shedding and reduction of the maximum pressure fluctuations and associated acoustic power. The arrangement and geometry were shown to be an important factor in determining leading-edge erosion, which was shown to increase at lower angles of attack.

The application of mVGs has started to be investigated in applications other than 2D hydrofoil. Examples include the study by Huang *et al.*¹⁸⁸ They investigated the effects of VGs on cavitation in marine shipping. The VGs studied could lead to more uniform wake and milder propeller cavitation. These VGs could decrease pressure fluctuations and cause a more uniform distribution of energy. Li *et al.*¹⁸⁹ designed a delta-shaped VG to solve the vibration problem in the hull propeller and improve the ship wake quality and uniformity. The VG design was based on the ship body lines. It improved the wake uniformity in certain positions as it could generate a more moderate circumference transition and effectively increase the velocity in high wake areas. Additionally, the VGs were able to smoothly transition the unsteady cavitation of the blade in circumference direction and decrease the amplitude of pressure fluctuations. The distance

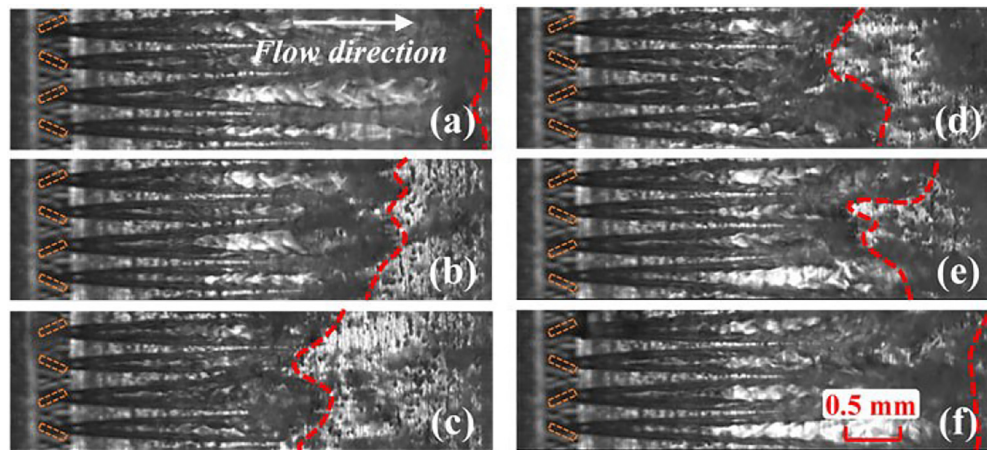


FIG. 24. (a)–(f) Dynamic behavior of vortex cavitation on a hydrofoil with micro-vortex generators, with dashed boxes and dashed lines indicating the position of vortex generators and the trailing edge of vortex cavitation, respectively. As shown in the picture, classical finger structures and Tollmien–Schlichting waves have been eliminated. The cavitation onset moved toward the leading edge, which happened at the laminar separation line for smooth hydrofoil. The onset cavitation mechanism includes stable vortex cavitation, which breaks down to a bubbly structure and accumulates in an attached cavity region.¹⁷¹ Reprinted with the permission from Che *et al.*, *Phys. Fluids* **31**, 044102 (2019). Copyright 2019 AIP Publishing.

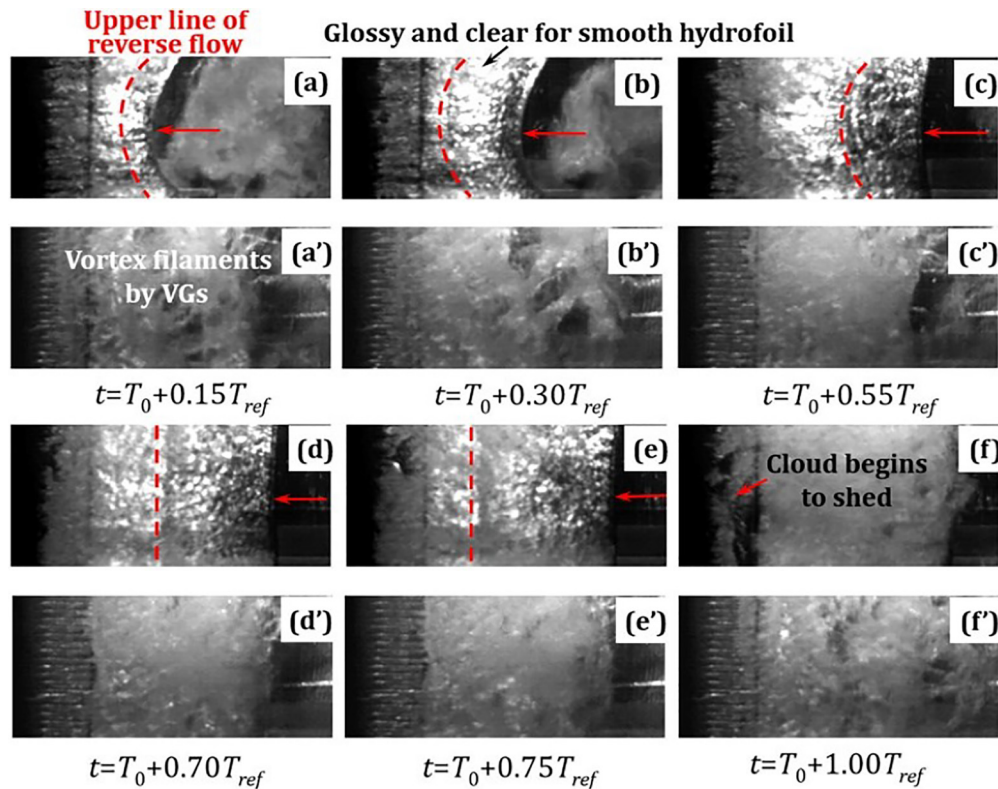


FIG. 25. Behavior of reentrant jets ($\alpha = 8^\circ$, $U_\infty = 10$ m/s, and $\sigma = 1.7$) on (a)–(f) smooth hydrofoil and (a')–(f') hydrofoil with vortex generators. For hydrofoil with vortex generators, downstream traveling vortices break the regular movements of re-entrant jets and suppress them. The cavity is confined and does not form a cloud, and the consequent collapse is not strong enough.¹⁸⁷ Reprinted with the permission from Qiu *et al.*, *Phys. Fluids* **32**, 104108 (2020). Copyright 2020 AIP Publishing.

between the positions of blade cavitation collapses, and ship bottom shell was increased after using VGs.

Teplov and Lomakin¹⁹⁰ used computation simulation to examine mVGs located at the front edge on the suction side of impeller blades in a centrifugal pump and analyzed their effect on the cavitation characteristics, efficiency, and pump head. The NPSH was significantly decreased, and the pump efficiency above the best efficiency point was increased.

A study published recently by Chen *et al.*¹⁹¹ investigated the effects on cavitation of two schematic designs of mVGs around a NACA66 hydrofoil. Two different sets of mVG were installed and positioned upstream of (mVG-1) and within (mVG-2) the laminar separation zone of the baseline hydrofoil. The experimental results indicated that the mVG-1 could promote inception of cavitation earlier than the baseline hydrofoil, while mVG-2 delayed cavitation inception especially at small angle of attack cases. Two reasons were suggested for the effect of the mVG-1. The mVG-1 modification was shown to generate fingerlike vortex at its rear, which was observed before in previous studies^{85,171,184} and is shown in Fig. 23. These vortices were responsible to induce fingerlike vortex cavitation. In addition, the mVG-1 increases the length of the laminar separation bubble (LSB), resulting in laminar boundary layer separation with a lower pressure minimum. Since mVG-2 was located in a high pressure zone from the leading-edge, there are insufficient downstream fingerlike

vortices to induce cavitation, which can reduce LSB length. Smaller LSB was able to suppress cavitation at $\alpha = 6^\circ$ – 8° . A summary of studies in the field of obstacles and VGs in cavitation control studies is presented in Table V.

IV. CONCLUSION

This study reviewed different passive flow control techniques with a focus on control cavitation application. The review of passive flow control devices in an aerodynamic application showed the potential of passive flow control methods in boundary layer separation, generating streamwise vortices in the boundary layer, transferring momentum near the wall, delaying the suppression of boundary layer separation, and the pressure recovery downstream of vortex generators. The vortex generators showed a better potential for controlling boundary layer separation than other passive flow control methods. Among different types of vortex generators, counter-rotating and co-rotating with $0.2 < h/\delta < 0.5$ and the distance of 5–30h from the upstream of baseline separation showed better effectiveness in controlling and suppressing boundary layer separation.

The review of passive flow control techniques in the hydraulic system shows the effectiveness of different cavitation control types in this method. Different studies in this field have proven the ability of passive flow control methods in suppressing and delaying boundary layer separation and reduction in cavity length and cavitation growth.

Many studies observed the generation of streamwise vortices and reduction in boundary layer spanwise non-uniformities. Moreover, transferring high momentum fluid from the free stream flow moved to the near-wall low energy region and moving higher kinetic energy flow to the surface's vicinity was another observation in these studies. Declining pressure gradient and intensity of pressure fluctuation at the separation point and increasing resistance against pressure rise before boundary layer separation are additional results of using passive flow control methods. As re-entrant jets play an important role in cavitation, the effect of passive flow control was weakening the re-entrant jets and their penetration depth and suppressing the propagation of the pressure wave of collapse. They are also effective in declining the recirculation zone thickness and, consequently, the velocity of re-entrant jets. In some experiments, passive flow control methods could delay cavitation inception, while there were some results with an earlier cavitation onset.

However, there is no study comparing different types of passive flow control under the same condition in controlling cavitation. In addition to all the effects mentioned above, vortex generators can eliminate classical "fingering structures" and Tollmien-Schlichting waves and affect partial cavity oscillation, transitional cavity oscillation, and the transition between these two instabilities. They are also effective in declining turbulent velocity fluctuation and decreasing cavitation erosion.

Few studies focused on the vortex generators in micro-scale.^{171,174,177,181,182,184,186} The most recent research in the field of vortex generators and its effect on the cavitation instabilities was based on the vane-type counter-rotating vortex generator with a minimum height of 0.05 mm (0.074 in manufacturing) with $h/\delta = 0.5$.^{171,184,186} According to single-phase flow studies of vortex generators, the most optimum h/δ range for vortex generators is $0.2 < h/\delta < 0.5$. Che *et al.*¹⁷¹ stated that because of manufacturing limits, they could not manufacture vortex generators with h/δ less than 0.74, and 3D printing could be a solution for manufacturing vortex generators of lower height and thinner thickness and might be relatively easy to be installed in fluid machinery.

According to this review, the potential and effectiveness of passive flow control, and specifically vortex generators, have been proven. However, there is great potential to optimize designs in terms of geometry, arrangement, and distance to the boundary layer separation. Since the major research in optimizing the design of vortex generators was based on the compressible single phase flow experiments and according to a different nature of compressible and multiphase flows in cavitation phenomenon, the analysis of optimized geometry criteria such as h/δ and l/h and $\Delta X_{VG}/h$ in hydraulic systems is necessary. Areas for additional investigation include manufacturing processes, including their lifetime and durability. Additionally, the specific application area of hydraulic systems, and particular centrifugal pumps, requires greater investigation due to the economic and sustainability gains, which might be realized from further optimization of these technologies.

ACKNOWLEDGMENTS

This work was funded by the European Union's Horizon 2020 research and innovation programme under Grant Agreement No. 862100 (NewSkin).

AUTHOR DECLARATIONS

Conflict of Interest

The authors have no conflicts of interest to disclose.

DATA AVAILABILITY

Data sharing is not applicable to this article as no new data were created or analyzed in this study.

REFERENCES

- J.-P. Franc and J.-M. Michel, *Fundamentals of Cavitation* (Springer Netherlands, 2005).
- Q. Wu, B. Huang, G. Wang, S. Cao, and M. Zhu, "Numerical modelling of unsteady cavitation and induced noise around a marine propeller," *Ocean Eng.* **160**, 143 (2018).
- D. Valentín, A. Presas, M. Egusquiza, C. Valero, and E. Egusquiza, "Transmission of high frequency vibrations in rotating systems. Application to cavitation detection in hydraulic turbines," *Appl. Sci.* **8**, 451 (2018).
- S. Mouvanal, D. Chatterjee, S. Bakshi, A. Burkhardt, and V. Mohr, "Numerical prediction of potential cavitation erosion in fuel injectors," *Int. J. Multiphase Flow* **104**, 113 (2018).
- Y. Hao and L. Tan, "Symmetrical and unsymmetrical tip clearances on cavitation performance and radial force of a mixed flow pump as turbine at pump mode," *Renewable Energy* **127**, 368 (2018).
- O. Reynolds, "The causes of the racing of the engines of screw steamers investigated theoretically and by experiment," *Trans. Inst. Naval Arch.* **14**, 56–57 (1873).
- R. E. A. Arndt, "Cavitation in fluid machinery and hydraulic structures," *Annu. Rev. Fluid Mech.* **13**, 273 (1981).
- A. J. Acosta, "Hydrofoils and hydrofoil craft," *Annu. Rev. Fluid Mech.* **5**, 161 (1973).
- C. E. Brennen, *Cavitating Flows* (Cambridge University Press, Cambridge, 2013).
- S. L. Ceccio and C. E. Brennen, "Observations of the dynamics and acoustics of travelling bubble cavitation," *J. Fluid Mech.* **233**, 633 (1991).
- R. W. Kermeen, *Water Tunnel Tests of NACA 4412 and Walchner Profile 7 Hydrofoils in Noncavitating and Cavitating Flows* (California Institute of Technology, 1956).
- H. Ganesh, S. A. Mäkiharju, and S. L. Ceccio, "Bubbly shock propagation as a mechanism for sheet-to-cloud transition of partial cavities," *J. Fluid Mech.* **802**, 37 (2016).
- M. van Rijsbergen, "A review of sheet cavitation inception mechanisms," in 16th International Symposium on Transport Phenomena and Dynamics of Rotating Machinery, Honolulu, USA (2016).
- E. Amromin, "Approximate analysis of hydrofoil material impact on cavitation inception," in 16th International Symposium on Transport Phenomena and Dynamics of Rotating Machinery (ISROMAC) Honolulu, USA (2016).
- M. Farhat, F. A. Gennoun, and F. O. Avellan, "The leading edge cavitation dynamics," in Fluids Engineering Division Summer Meeting (2002).
- E. Ezzatneshan, "Study of surface wettability effect on cavitation inception by implementation of the lattice Boltzmann method," *Phys. Fluids* **29**, 113304 (2017).
- T. F. Groß and P. F. Pelz, "Diffusion-driven nucleation from surface nuclei in hydrodynamic cavitation," *J. Fluid Mech.* **830**, 138 (2017).
- V. H. Arakeri, "Viscous effects on the position of cavitation separation from smooth bodies," *J. Fluid Mech.* **68**, 779 (1975).
- A. T. Leger and S. L. Ceccio, "Examination of the flow near the leading edge of attached cavitation. Part 1. Detachment of two-dimensional and axisymmetric cavities," *J. Fluid Mech.* **376**, 61 (1998).
- V. H. Arakeri and A. J. Acosta, "Viscous effects in the inception of cavitation on axisymmetric bodies," *J. Fluids Eng.* **95**, 519 (1973).
- J. P. Franc and J. M. Michel, "Attached cavitation and the boundary layer: Experimental investigation and numerical treatment," *J. Fluid Mech.* **154**, 63 (1985).
- S. Scott Collis, R. D. Joslin, A. Seifert, and V. Theofilis, "Issues in active flow control: Theory, control, simulation, and experiment," *Prog. Aerosp. Sci.* **40**, 237 (2004).

- ²³M. Gad-el-Hak, *Flow Control: Passive, Active, and Reactive Flow Management* (Cambridge University Press, Cambridge, 2000).
- ²⁴T. Moghaddam and N. B. Neishabouri, "On the active and passive flow separation control techniques over airfoils," *IOP Conf. Ser.* **248**, 012009 (2017).
- ²⁵M. Genç, K. Koca, H. Demir, and H. Açıkel, "Traditional and new types of passive flow control techniques to pave the way for high maneuverability and low structural weight for UAVs and MAVs," in *Autonomous Vehicles* (IntechOpen, 2020).
- ²⁶J. C. Lin, "Review of research on low-profile vortex generators to control boundary-layer separation," *Prog. Aerosp. Sci.* **38**, 389 (2002).
- ²⁷L. Howarth and G. I. Taylor, "Concerning the effect of compressibility on laminar boundary layers and their separation," *Proc. R. Soc. London, Ser. A* **194**, 16 (1948).
- ²⁸K. Stewartson, "Correlated incompressible and compressible boundary layers," *Proc. R. Soc. London, Ser. A* **200**, 84 (1949).
- ²⁹O. Lögdberg, "Vortex generators and turbulent boundary layer separation control," Licentiate thesis (KTH, 2006).
- ³⁰B. Munson, D. Young, and T. Okiishi, *Fundamentals of Fluid Mechanics* (John Wiley and Sons, 2002).
- ³¹NASA, *Drag of a Sphere* (NASA, Glenn Research Center); available at <https://www.grc.nasa.gov/www/k-12/airplane/shaped.html>
- ³²M. S. Genç, U. Kaynak, and G. D. Lock, "Flow over an aerofoil without and with a leading-edge slat at a transitional Reynolds number," *Proc. Inst. Mech. Eng., Part G* **223**, 217 (2009).
- ³³L. Traub and M. Kaula, "Effect of leading-edge slats at low Reynolds numbers," *Aerospace* **3**, 39 (2016).
- ³⁴G. Pechlivanoglou, "Passive and active flow control solutions for wind turbine blades," Ph.D. thesis (Technische Universität Berlin, 2013).
- ³⁵Z. Wang and M. Zhuang, "Leading-edge serrations for performance improvement on a vertical-axis wind turbine at low tip-speed-ratios," *Appl. Energy* **208**, 1184 (2017).
- ³⁶S. Beyhaghi and R. S. Amano, "A parametric study on leading-edge slots used on wind turbine airfoils at various angles of attack," *J. Wind Eng. Ind. Aerodyn.* **175**, 43 (2018).
- ³⁷G. Godard and M. Stanislas, "Control of a decelerating boundary layer. Part 1: Optimization of passive vortex generators," *Aerosp. Sci. Technol.* **10**, 181 (2006).
- ³⁸A. S. Shehata, Q. Xiao, K. M. Saqr, A. Naguib, and D. Alexander, "Passive flow control for aerodynamic performance enhancement of airfoil with its application in Wells turbine: Under oscillating flow condition," *Ocean Eng.* **136**, 31 (2017).
- ³⁹W. W. Huebsch, *Numerical Investigation on the Interaction Between Surface Roughness and Viscous Flows* (Iowa State University, 2000).
- ⁴⁰M. S. Genç, K. Koca, and H. H. Açıkel, "Investigation of pre-stall flow control on wind turbine blade airfoil using roughness element," *Energy* **176**, 320 (2019).
- ⁴¹K. Koca, M. S. Genç, H. H. Açıkel, M. Çağdaş, and T. M. Bodur, "Identification of flow phenomena over NACA 4412 wind turbine airfoil at low Reynolds numbers and role of laminar separation bubble on flow evolution," *Energy* **144**, 750 (2018).
- ⁴²M. S. Genç, K. Koca, H. H. Açıkel, G. Özkan, M. S. Kırış, and R. Yıldız, "Flow characteristics over NACA4412 airfoil at low Reynolds number," *EPJ Web Conf.* **114**, 02029 (2016).
- ⁴³M. Gad-el-Hak, "Modern developments in flow control," *Appl. Mech. Rev.* **49**, 365 (1996).
- ⁴⁴A. M. Kuethe, "Effect of streamwise vortices on wake properties associated with sound generation," *J. Aircr.* **9**, 715 (1972).
- ⁴⁵D. Rao and T. Kariya, *Boundary-Layer Submerged Vortex Generators for Separation Control: An Exploratory Study* (American Institute of Aeronautics and Astronautics, 1988).
- ⁴⁶J. C. Lin, F. G. Howard, and G. V. Selby, "Small submerged vortex generators for turbulent flow separation control," *J. Spacecr. Rockets* **27**, 503 (1990).
- ⁴⁷J. Lin, F. Howard, and G. Selby, *Exploratory Study of Vortex-Generating Devices for Turbulent Flow Separation Control* (American Institute of Aeronautics and Astronautics, 1991).
- ⁴⁸M. Kerho, S. Hutcherson, R. F. Blackwelder, and R. H. Liebeck, "Vortex generators used to control laminar separation bubbles," *J. Aircr.* **30**, 315 (1993).
- ⁴⁹J. Lin, F. Howard, D. Bushnell, and G. Selby, *Investigation of Several Passive and Active Methods for Turbulent Flow Separation Control* (American Institute of Aeronautics and Astronautics, 1990).
- ⁵⁰J. Lin, *Control of Turbulent Boundary-Layer Separation Using Micro-Vortex Generators* (American Institute of Aeronautics and Astronautics, 1999).
- ⁵¹S. Gorton, L. Jenkins, and S. Anders, *Flow Control Device Evaluation for An Internal Flow With An Adverse Pressure Gradient* (American Institute of Aeronautics and Astronautics, 2002).
- ⁵²J. C. Lin, S. K. Robinson, R. J. McGhee, and W. O. Valarezo, "Separation control on high-lift airfoils via micro-vortex generators," *J. Aircr.* **31**, 1317 (1994).
- ⁵³T. Tai, *Effect of Micro-Vortex Generators on V-22 Aircraft Forward-Flight Aerodynamics* (American Institute of Aeronautics and Astronautics, 2002).
- ⁵⁴P. Ashill, J. Fulker, and K. Hackett, *Studies of Flows Induced by Sub Boundary Layer Vortex Generators (SBVGs)* (American Institute of Aeronautics and Astronautics, 2002).
- ⁵⁵P. Ashill, J. Fulker, and K. Hackett, *Research at DERA on Sub Boundary Layer Vortex Generators (SBVGs)* (American Institute of Aeronautics and Astronautics, 2001).
- ⁵⁶J. W. Hamstra, D. N. Miller, P. P. Truax, B. A. Anderson, and B. J. Wendt, "Active inlet flow control technology demonstration," *Aeronaut. J.* **104**, 473 (2000).
- ⁵⁷C. Yao, J. Lin, and B. Allen, *Flowfield Measurement of Device-Induced Embedded Streamwise Vortex on a Flat Plate* (American Institute of Aeronautics and Astronautics, 2002).
- ⁵⁸B. Allan, C.-S. Yao, and J. Lin, *Numerical Simulations of Vortex Generator Vanes and Jets on a Flat Plate* (American Institute of Aeronautics and Astronautics, 2002).
- ⁵⁹H. Holden and H. Babinsky, *Vortex Generators Near Shock/Boundary Layer Interactions* (American Institute of Aeronautics and Astronautics, 2004).
- ⁶⁰H. Babinsky, Y. Li, and C. W. P. Ford, "Microramp control of supersonic oblique shock-wave/boundary-layer interactions," *AIAA J.* **47**, 668 (2009).
- ⁶¹S. Ghosh, J.-I. Choi, and J. R. Edwards, "Numerical simulations of effects of micro vortex generators using immersed-boundary methods," *AIAA J.* **48**, 92 (2010).
- ⁶²X. Dong, Y. Chen, G. Dong, and Y. Liu, "Study on wake structure characteristics of a slotted micro-ramp with large-eddy simulation," *Fluid Dyn. Res.* **49**, 035507 (2017).
- ⁶³Z. Sun, F. Schrijer, F. Scarano, and B. Oudheusden, "Decay of the supersonic turbulent wakes from micro-ramps," *Phys. Fluids* **26**, 025115 (2014).
- ⁶⁴Q. Li and C. Liu, *LES for Supersonic Ramp Control Flow Using MVG at $M = 2.5$ and $Re_\theta = 1440$* (American Institute of Aeronautics and Astronautics, 2010).
- ⁶⁵Z. Sun, F. F. J. Schrijer, F. Scarano, and B. W. van Oudheusden, "The three-dimensional flow organization past a micro-ramp in a supersonic boundary layer," *Phys. Fluids* **24**, 055105 (2012).
- ⁶⁶D. Sun, J. Chen, C. Li, P. Liu, Q. Guo, and X. Yuan, "On the wake structure of a micro-ramp vortex generator in hypersonic flow," *Phys. Fluids* **32**, 126111 (2020).
- ⁶⁷D. Sun, Q. Guo, C. Li, and P. Liu, "Direct numerical simulation of effects of a micro-ramp on a hypersonic shock wave/boundary layer interaction," *Phys. Fluids* **31**, 126101 (2019).
- ⁶⁸M. Z. Akhter and F. K. Omar, "Review of flow-control devices for wind-turbine performance enhancement," *Energies* **14**, 1268 (2021).
- ⁶⁹J. Franc, *Physics and Control of Cavitation* (University of Grenoble LEGI, 2008).
- ⁷⁰Q. Chen, Y. Liu, Q. Wu, Y. Wang, T. Liu, and G. Wang, "Global cavitation patterns and corresponding hydrodynamics of the hydrofoil with leading edge roughness," *Acta Mech. Sin.* **36**, 1202 (2020).
- ⁷¹O. De La Torre, X. Escaler, E. Eguisquiza, and M. Farhat, "Experimental investigation of added mass effects on a hydrofoil under cavitation conditions," *J. Fluids Struct.* **39**, 173 (2013).
- ⁷²M. Kadivar, D. Tormey, and G. McGranaghan, "A review on turbulent flow over rough surfaces: Fundamentals and theories," *Int. J. Thermofluids* **10**, 100077 (2021).
- ⁷³H. L. Dryden, "Review of published data on the effect of roughness on transition from laminar to turbulent flow," *J. Aeronaut. Sci.* **20**, 477 (1953).

- ⁷⁴M. F. Kerho and M. B. Bragg, "Airfoil boundary-layer development and transition with large leading-edge roughness," *AIAA J.* **35**, 75 (1997).
- ⁷⁵B. Stutz, "Influence of roughness on the two-phase flow structure of sheet cavitation," *J. Fluids Eng.* **125**, 652 (2003).
- ⁷⁶O. Coutier-Delgosha, J.-F. Devillers, M. Leriche, and T. Pichon, "Effect of wall roughness on the dynamics of unsteady cavitation," *J. Fluids Eng.* **127**, 726 (2005).
- ⁷⁷P. Ausoni, M. Farhat, and F. Avellan, "Hydrofoil roughness effects on von Kármán vortex shedding," in 2nd IAHR International Meeting of the Workgroup on Cavitation and Dynamic Problems in Hydraulic Machinery and Systems (2007).
- ⁷⁸P. Ausoni, A. Zobeiri, F. Avellan, and M. Farhat, "The effects of a tripped turbulent boundary layer on vortex shedding from a blunt trailing edge hydrofoil," *J. Fluids Eng.* **134**, 051207 (2012).
- ⁷⁹P. L. Delafin, F. Deniset, and J. A. Astolfi, "Effect of the laminar separation bubble induced transition on the hydrodynamic performance of a hydrofoil," *Eur. J. Mech.-B/Fluids* **46**, 190 (2014).
- ⁸⁰M. Petkovšek, H. Hočvar, and P. Gregorčič, *Cavitation Dynamics on Laser-Textured Surfaces* (ASME Press, 2018).
- ⁸¹A. M. Emelyanenko, F. M. Shagieva, A. G. Domantovsky, and L. B. Boinovich, "Nanosecond laser micro- and nanotexturing for the design of a superhydrophobic coating robust against long-term contact with water, cavitation, and abrasion," *Appl. Surf. Sci.* **332**, 513 (2015).
- ⁸²R. Tao, R. F. Xiao, and F. Mohamed, "Effect of leading edge roughness on cavitation inception and development on thin hydrofoil," *J. Drain. Irrig. Mach. Eng.* **35**(11), 921–926, 940 (2017).
- ⁸³S. A. Churkin, K. S. Pervunin, A. Y. Kravtsova, D. M. Markovich, and K. Hanjalić, "Cavitation on NACA0015 hydrofoils with different wall roughness: High-speed visualization of the surface texture effects," *J. Visualization* **19**, 587 (2016).
- ⁸⁴K. Onishi, K. Matsuda, and K. Miyagawa, "Influence of hydrophilic and hydrophobic coating on hydrofoil performance," in International Symposium on Transport Phenomena and Dynamics of Rotating Machinery (ISROMAC) (2017).
- ⁸⁵J. Hao, M. Zhang, and X. Huang, "The influence of surface roughness on cloud cavitation flow around hydrofoils," *Acta Mech. Sin.* **34**, 10 (2018).
- ⁸⁶A. Asnaghi, U. Svennberg, R. Gustafsson, and R. E. Bensow, "Investigations of tip vortex mitigation by using roughness," *Phys. Fluids* **32**, 065111 (2020).
- ⁸⁷U. Svennberg, A. Asnaghi, R. Gustafsson, and R. Bensow, "Experimental analysis of tip vortex cavitation mitigation by controlled surface roughness," *J. Hydrodyn.* **32**, 1059 (2020).
- ⁸⁸X. Lv, W. T. Wu, J. Lv, K. Mao, L. Gao, and Y. Li, "Study on the law of pseudo-cavitation on superhydrophobic surface in turbulent flow field of backward-facing step," *Fluids* **6**, 200 (2021).
- ⁸⁹H. Kim and C. Kim, "A physics-based cavitation model ranging from inertial to thermal regimes," *Int. J. Heat Mass Transfer* **181**, 121991 (2021).
- ⁹⁰M. Adama Maiga, O. Coutier-Delgosha, and D. Buisine, "A new cavitation model based on bubble-bubble interactions," *Phys. Fluids* **30**, 123301 (2018).
- ⁹¹O. Ivashnev, M. Ivashneva, and N. Smirnov, "Rarefaction waves in nonequilibrium-boiling fluid flows," *Fluid Dyn.* **35**, 485 (2000).
- ⁹²A. A. Aganin and T. F. Khalitova, "Calculation of small deformations of a radially convergent shock wave inside a cavitation bubble," *Lobachevskii J. Math.* **42**, 1954 (2021).
- ⁹³M. Zhang, Q. Chang, X. Ma, G. Wang, and B. Huang, "Physical investigation of the counterjet dynamics during the bubble rebound," *Ultrason. Sonochem.* **58**, 104706 (2019).
- ⁹⁴A. A. Aganin, A. I. Davletshin, and T. F. Khalitova, "Expansion and collapse of bubbles in the central region of a streamer," *Lobachevskii J. Math.* **42**, 15 (2021).
- ⁹⁵O. Ivashnyov, M. Ivashneva, and N. Smirnov, "Slow waves of boiling under hot water depressurization," *J. Fluid Mech.* **413**, 149 (2000).
- ⁹⁶X. Tang, X. Duan, H. Gao, X. Li, and X. Shi, "CFD investigations of transient cavitation flows in pipeline based on weakly-compressible model," *Water* **12**, 448 (2020).
- ⁹⁷V. K. Kedrinskiy and E. S. Zhuravleva, "Formation of a cavitation zone behind a rarefaction wave front in a shock-loaded thin layer of a multiphase liquid," *J. Phys.* **1268**, 012032 (2019).
- ⁹⁸A. Fraters, M. Van Den Berg, Y. De Loore, H. Reinten, H. Wijshoff, D. Lohse, M. Versluis, and T. Segers, "Inkjet nozzle failure by heterogeneous nucleation: Bubble entrainment, cavitation, and diffusive growth," *Phys. Rev. Appl.* **12**, 064019 (2019).
- ⁹⁹E. S. Zhuravleva and V. K. Kedrinskiy, "Focusing of the rarefaction wave in a thin cavitating fluid layer with a free boundary," *J. Appl. Mech. Tech. Phys.* **59**, 1004 (2018).
- ¹⁰⁰N. Kyriazis, P. Koukouvinis, and M. Gavaises, "Modelling cavitation during drop impact on solid surfaces," *Adv. Colloid Interface Sci.* **260**, 46 (2018).
- ¹⁰¹O. E. Ivashnyov and N. N. Smirnov, "Thermal growth of a vapor bubble moving in superheated liquid," *Phys. Fluids* **16**, 809 (2004).
- ¹⁰²R. I. Nigmatulin, J. R. T. Lahey, R. P. Taleyarkhan, C. D. West, and R. C. Block, "On thermonuclear processes in cavitation bubbles," *Phys.-Usp.* **57**, 877 (2014).
- ¹⁰³Y. Liu and Y. Peng, "Study on the collapse process of cavitation bubbles including heat transfer by lattice Boltzmann method," *J. Mar. Sci. Eng.* **9**, 219 (2021).
- ¹⁰⁴M. Gallo, F. Magaletti, D. Cocco, and C. M. Casciola, "Nucleation and growth dynamics of vapour bubbles," *J. Fluid Mech.* **883**, A14 (2020).
- ¹⁰⁵J. Zhu, S. Wang, and X. Zhang, "Influences of thermal effects on cavitation dynamics in liquid nitrogen through venturi tube," *Phys. Fluids* **32**, 012105 (2020).
- ¹⁰⁶D. Papoulias and M. Gavaises, "Modelling of single bubble-dynamics and thermal effects," *J. Phys.* **656**, 012098 (2015).
- ¹⁰⁷M. T. Warnez and E. Johnsen, "Numerical modeling of bubble dynamics in viscoelastic media with relaxation," *Phys. Fluids* **27**, 063103 (2015).
- ¹⁰⁸A. A. Aganin, O. R. Ganiev, A. I. Davletshin, and L. E. Ukrainskii, "Evaluation of thermal and acoustic energy during collapse of cavitation bubbles," *J. Mach. Manuf. Reliab.* **49**, 367 (2020).
- ¹⁰⁹A. A. Aganin, O. R. Ganiev, A. I. Davletshin, and L. E. Ukrainskiy, "Liquid heating during the collapse of a single cavitation bubble," *J. Mach. Manuf. Reliab.* **49**, 24 (2020).
- ¹¹⁰R. I. Nigmatulin, A. A. Aganin, and D. Y. Toporkov, "Possibility of cavitation bubble supercompression in tetradecane," *Dokl. Phys.* **63**, 348 (2018).
- ¹¹¹A. A. Aganin and T. F. Khalitova, "Small non-sphericity of a convergent shock wave arising in a cavitation bubble in acetone during its collapse," *J. Phys.* **1588**, 012058 (2020).
- ¹¹²A. A. Aganin, M. A. Il'gamov, R. I. Nigmatulin, and D. Y. Toporkov, "Evolution of distortions of the spherical shape of a cavitation bubble in acoustic supercompression," *Fluid Dyn.* **45**, 50 (2010).
- ¹¹³S. Park and G. Son, "Numerical study of the effect of liquid compressibility on acoustic droplet vaporization," *Ultrason. Sonochem.* **79**, 105769 (2021).
- ¹¹⁴Y. H. Chen, J. M. Zhan, and Y. T. Li, "Numerical simulation of cavitation-bubble expansion and collapse inside a bottle subjected to impact on its top-side," *Eng. Appl. Comput. Fluid Mech.* **15**, 1440 (2021).
- ¹¹⁵F. Denner, "The Gilmore-NASG model to predict single-bubble cavitation in compressible liquids," *Ultrason. Sonochem.* **70**, 105307 (2021).
- ¹¹⁶R. F. Ganiev, A. A. Aganin, O. R. Ganiev, G. N. Granova, A. I. Davletshin, L. E. Ukrainskii, and I. G. Ustenko, "Compression of cavitation bubble in viscous liquid," *J. Mach. Manuf. Reliab.* **46**, 1 (2017).
- ¹¹⁷M. Sivčák and T. Hruš, "Influence of bubbles in the shock liquid at its compressibility," in *Advances in Mechanism Design II* (Springer, 2017).
- ¹¹⁸T. Trummler, S. J. Schmidt, and N. A. Adams, "Numerical investigation of non-condensable gas effect on vapor bubble collapse," *Phys. Fluids* **33**, 096107 (2021).
- ¹¹⁹U. Iben, A. Makhnov, and A. Schmidt, "Numerical investigation of cavitating flows with liquid degassing," *J. Phys.* **1038**, 012128 (2018).
- ¹²⁰J. Lee, "Importance of sonication and solution conditions on the acoustic cavitation activity," in *Handbook of Ultrasonics and Sonochemistry* (Springer, 2016).
- ¹²¹E. Kadivar, O. el Moctar, R. Skoda, and U. Löschner, "Experimental study of the control of cavitation-induced erosion created by collapse of single bubbles using a micro structured riblet," *Wear* **486–487**, 204087 (2021).
- ¹²²S. R. Gonzalez-Avila, D. M. Nguyen, S. Arunachalam, E. M. Domingues, H. Mishra, and C.-D. Ohl, "Mitigating cavitation erosion using biomimetic gas-entrapping microtextured surfaces (GEMS)," *Sci. Adv.* **6**, eaax6192 (2020).

- ¹²³Y. T. Shen and R. Eppler, "Wing sections for hydrofoils—part 2: Nonsymmetrical profiles," *J. Ship Res.* **25**, 191 (1981).
- ¹²⁴Y. T. Shen, "Wing sections for hydrofoils—Part 3: Experimental verifications," *J. Ship Res.* **29**, 39 (1985).
- ¹²⁵S. Kyparissis and D. Margaris, "Experimental investigation of cavitation in a centrifugal pump with double-arc synthetic blade design method," *Int. Rev. Mech. Eng.* **5**, 884 (2011).
- ¹²⁶S. D. Kyparissis and D. P. Margaris, "Experimental investigation and passive flow control of a cavitating centrifugal pump," *Int. J. Rotating Mach.* **2012**, 248082.
- ¹²⁷W. Shi, M. Atlar, R. Rosli, B. Aktas, and R. Norman, "Cavitation observations and noise measurements of horizontal axis tidal turbines with biomimetic blade leading-edge designs," *Ocean Eng.* **121**, 143 (2016).
- ¹²⁸C. B. Senel, H. Maral, L. A. Kavurmacioglu, and C. Camci, "An aerothermal study of the influence of squealer width and height near a HP turbine blade," *Int. J. Heat Mass Transfer* **120**, 18 (2018).
- ¹²⁹C. Camci, D. Dey, and L. Kavurmacioglu, "Aerodynamics of tip leakage flows near partial squealer rims in an axial flow turbine stage," *J. Turbomach.* **127**, 14 (2005).
- ¹³⁰J. H. Cheon and S. W. Lee, "Tip leakage aerodynamics over the cavity squealer tip equipped with full coverage winglets in a turbine cascade," *Int. J. Heat Fluid Flow* **56**, 60 (2015).
- ¹³¹M. Lei and Z. Junwei, *Effects of Blade Tip Foil Thickening on Tip Vortexes in Ducted Propeller* (Atlantis Press, 2015).
- ¹³²Q. Guo, L. Zhou, and Z. Wang, "Numerical evaluation of the clearance geometries effect on the flow field and performance of a hydrofoil," *Renewable Energy* **99**, 390 (2016).
- ¹³³S. Q. Wu, W. D. Shi, D. S. Zhang, J. Yao, and C. Cheng, "Influence of blade tip rounding on tip leakage vortex cavitation of axial flow pump," *IOP Conf. Ser.* **52**, 062011 (2013).
- ¹³⁴Y. Liu and L. Tan, "Method of C groove on vortex suppression and energy performance improvement for a NACA0009 hydrofoil with tip clearance in tidal energy," *Energy* **155**, 448 (2018).
- ¹³⁵D. Kang, Y. Arimoto, K. Yonezawa, H. Horiguchi, Y. Kawata, C. Hah, and Y. Tsujimoto, "Suppression of cavitation instabilities in an inducer by circumferential groove and explanation of higher frequency components," *Int. J. Fluid Mach. Syst.* **3**, 137 (2010).
- ¹³⁶M. Dreyer, *Mind The Gap: Tip Leakage Vortex Dynamics and Cavitation in Axial Turbines* (École Polytechnique Fédérale De Lausanne, 2015).
- ¹³⁷H-y Cheng, B. Ji, X-p Long, and M. Farhat, "A review of cavitation in tip-leakage flow and its control," *J. Hydrodyn.* **33**, 226 (2021).
- ¹³⁸D. Custodio, C. Henocho, and H. Johari, "Cavitation on hydrofoils with leading edge protuberances," *Ocean Eng.* **162**, 196 (2018).
- ¹³⁹W. G. Zhao and G. Wang, "Research on passive control of cloud cavitation based on a bionic fin-fin structure," *Eng. Comput.* **37**, 863 (2019).
- ¹⁴⁰R. Kant and A. Bhattacharyya, "A bio-inspired twin-protuberance hydrofoil design," *Ocean Eng.* **218**, 108209 (2020).
- ¹⁴¹D. Li, Q. Yang, W. Yang, H. Chang, and H. Wang, "Bionic leading-edge protuberances and hydrofoil cavitation," *Phys. Fluids* **33**, 093317 (2021).
- ¹⁴²J. Li, C. Liu, and X. Li, "Effects of wavy leading-edge protuberance on hydrofoil performance and its flow mechanism," *J. Mar. Sci. Eng.* **9**, 1138 (2021).
- ¹⁴³R. García-Mayoral and J. Jiménez, "Drag reduction by riblets," *Philos. Trans. R. Soc. A* **369**, 1412 (2011).
- ¹⁴⁴W. Li, W. Jessen, D. Roggenkamp, M. Klaas, W. Silex, M. Schiek, and W. Schröder, "Turbulent drag reduction by spanwise traveling ribbed surface waves," *Eur. J. Mech.-B/Fluids* **53**, 101 (2015).
- ¹⁴⁵F. E. Fish and G. V. Lauder, "Passive and active flow control by swimming fishes and mammals," *Annu. Rev. Fluid Mech.* **38**, 193 (2006).
- ¹⁴⁶Y. Li, H. Chen, J. Wang, and D. Chen, "Effect of grooves on cavitation around the body of revolution," *J. Fluids Eng.* **132**, 011301 (2009).
- ¹⁴⁷A. Danlos, F. Ravelet, O. Coutier-Delgosha, and F. Bakir, "Cavitation regime detection through proper orthogonal decomposition: Dynamics analysis of the sheet cavity on a grooved convergent-divergent nozzle," *Int. J. Heat Fluid Flow* **47**, 9 (2014).
- ¹⁴⁸A. Danlos, J.-E. Méhal, F. Ravelet, O. Coutier-Delgosha, and F. Bakir, "Study of the cavitating instability on a grooved venturi profile," *J. Fluids Eng.* **136**, 101302 (2014).
- ¹⁴⁹Y. Xu, L. Tan, Y. Liu, and S. Cao, "Pressure fluctuation and flow pattern of a mixed-flow pump with different blade tip clearances under cavitation condition," *Advances in Mechanical Engineering* **9** (2017).
- ¹⁵⁰H. Cheng, X. Long, B. Ji, X. Peng, and M. Farhat, "Suppressing tip-leakage vortex cavitation by overhanging grooves," *Exp. Fluids* **61**, 159 (2020).
- ¹⁵¹H. Kato, H. Yamaguchi, S. Okada, K. Kikuchi, and M. Miyanaga, "Suppression of sheet cavitation inception by water discharge through slit," *J. Fluids Eng.* **109**, 70 (1987).
- ¹⁵²R. E. A. Arndt, C. R. Ellis, and S. Paul, "Preliminary investigation of the use of air injection to mitigate cavitation erosion," *J. Fluids Eng.* **117**, 498 (1995).
- ¹⁵³K. N. O. David Japikse and D. O. Baun, "Stability enhancement of compressors and turbopumps by passive flow control," Technical Report No. TFAWS06-1040 (2006).
- ¹⁵⁴B. Zhu, H. Chen, and Q. Wei, "Numerical and experimental investigation of cavitating characteristics in centrifugal pump with gap impeller," *Int. J. Turbo Jet Eng.* **31**, 187 (2014).
- ¹⁵⁵Z. Bing and C. Hongxun, "Analysis of the staggered and fixed cavitation phenomenon observed in centrifugal pumps employing a gap drainage impeller," *J. Fluids Eng.* **139**, 031301 (2016).
- ¹⁵⁶Y. Kamikura, H. Kobayashi, S. Kawasaki, and Y. Iga, "Three dimensional numerical analysis of inducer about suppression of cavitation instabilities by asymmetric slits on blades," *IOP Conf. Ser.* **240**, 032044 (2019).
- ¹⁵⁷W. Wang, Q. Yi, S. Lu, and X. Wang, "Exploration and research of the impact of hydrofoil surface water injection on cavitation suppression," in Turbo Expo: Power for Land, Sea, and Air (2017).
- ¹⁵⁸Y. Kawanami, H. Kato, H. Yamaguchi, M. Tanimura, and Y. Tagaya, "Mechanism and control of cloud cavitation," *J. Fluids Eng.* **119**, 788 (1997).
- ¹⁵⁹T. Pham, F. Larrarte, and D. Fruman, "Investigation of unsteady sheet cavitation and cloud cavitation mechanisms," *J. Fluids Eng.* **121**, 289 (1999).
- ¹⁶⁰K. Sato, M. Tanada, S. Monden, and Y. Tsujimoto, "Observations of oscillating cavitation on a flat plate hydrofoil," *JSME Int. J. Ser. B* **45**, 646 (2002).
- ¹⁶¹W.-G. Zhao, L.-X. Zhang, X.-M. Shao, and J. Deng, "Numerical study on the control mechanism of cloud cavitation by obstacles," *J. Hydrodyn., Ser. B* **22**, 792 (2010).
- ¹⁶²H. Ganesh, S. Mäkiharju, and S. Ceccio, "Interaction of a compressible bubbly flow with an obstacle placed within a shedding partial cavity," *J. Phys.* **656**, 012151 (2015).
- ¹⁶³S. Watanabe, N. Enomoto, K. Ishizaka, A. Furukawa, and J.-H. Kim, "Suppression of cavitation surge of a helical inducer occurring in partial flow conditions," *Turbomachinery* **32**, 94 (2004).
- ¹⁶⁴J.-H. Kim, K. Ishizaka, S. Watanabe, and A. Furukawa, "Cavitation surge suppression of pump inducer with axi-asymmetrical inlet plate," *Int. J. Fluid Mach. Syst.* **3**, 50 (2010).
- ¹⁶⁵J. Huang, C. Yu, Y. Wang, C. Xu, and C. Huang, "Passive control of cavitating flow around an axisymmetric projectile by using a trip bar," *Theor. Appl. Mech. Lett.* **7**, 181 (2017).
- ¹⁶⁶E. Kadivar, E. Kadivar, K. Javadi, and S. M. Javadpour, "The investigation of natural super-cavitation flow behind three-dimensional cavitators: Full cavitation model," *Appl. Math. Modell.* **45**, 165 (2017).
- ¹⁶⁷B. Che, L. Cao, N. Chu, D. Likhachev, and D. Wu, "Effect of obstacle position on attached cavitation control through response surface methodology," *J. Mech. Sci. Technol.* **33**, 4265 (2019).
- ¹⁶⁸L. Zhang, M. Chen, and X. Shao, "Inhibition of cloud cavitation on a flat hydrofoil through the placement of an obstacle," *Ocean Eng.* **155**, 1–9 (2018).
- ¹⁶⁹G. Zhao, L. Cao, B. Che, R. Wu, S. Yang, and D. Wu, "Towards the control of blade cavitation in a waterjet pump with inlet guide vanes: Passive control by obstacles," *Ocean Eng.* **231**, 108820 (2021).
- ¹⁷⁰Z. Lin, J. Tao, D. Yin, and Z. Zhu, "Numerical study on cavitation over flat hydrofoils with arc obstacles," *Phys. Fluids* **33**, 085101 (2021).
- ¹⁷¹B. Che, N. Chu, S. J. Schmidt, L. Cao, D. Likhachev, and D. Wu, "Control effect of micro vortex generators on leading edge of attached cavitation," *Phys. Fluids* **31**, 044102 (2019).
- ¹⁷²H. An, "On the use of vortex generators to control cavitation in a backward facing step flow," Ph.D. thesis (Purdue University, 2007).
- ¹⁷³Y. Liang-mei, "Application of the vortex generator to control the PHV cavitation," *J. Ship Mech.* **13**, 873 (2009).

- ¹⁷⁴K. Javadi, M. M. Dorostkar, and A. Katal, "Cavitation passive control on immersed bodies," *J. Mar. Sci. Appl.* **16**, 33 (2017).
- ¹⁷⁵A. Amini, M. Reclari, T. Sano, M. Iino, and M. Farhat, "Suppressing tip vortex cavitation by winglets," *Exp. Fluids* **60**, 159 (2019).
- ¹⁷⁶V. C. Andichamy, G. T. Khokhar, and C. Camci, "An experimental study of using vortex generators as tip leakage flow interrupters in an axial flow turbine stage," in *Turbo Expo: Power for Land, Sea, and Air* (2018).
- ¹⁷⁷E. Kadivar, O. E. Moctar, and K. Javadi, "Investigation of the effect of cavitation passive control on the dynamics of unsteady cloud cavitation," *Appl. Math. Modell.* **64**, 333 (2018).
- ¹⁷⁸E. Kadivar, M. V. Timoshevskiy, M. Y. Nichik, O. el Moctar, T. E. Schellin, and K. S. Pervunin, "Control of unsteady partial cavitation and cloud cavitation in marine engineering and hydraulic systems," *Phys. Fluids* **32**, 052108 (2020).
- ¹⁷⁹E. Kadivar, M. V. Timoshevskiy, K. S. Pervunin, and O. El Moctar, "Experimental and numerical study of the cavitation surge passive control around a semi-circular leading-edge flat plate," *J. Mar. Sci. Technol.* **25**, 1010 (2020).
- ¹⁸⁰C. Xu and B. C. Khoo, "Dynamics of the supercavitating hydrofoil with cavitation in steady flow field," *Phys. Fluids* **32**, 123307 (2020).
- ¹⁸¹E. Kadivar, O. El Moctar, and K. Javadi, "Stabilization of cloud cavitation instabilities using cylindrical cavitating-bubble generators (CCGs)," *Int. J. Multiphase Flow* **115**, 108 (2019).
- ¹⁸²E. Kadivar, M. Timoshevskiy, K. Pervunin, and O. El Moctar, "Experimental investigation of the passive control of unsteady cloud cavitation using miniature vortex generators (MVGs)," *IOP Conf. Ser.* **405**, 012002 (2019).
- ¹⁸³E. Kadivar, M. V. Timoshevskiy, K. S. Pervunin, and O. El Moctar, "Cavitation control using cylindrical cavitating-bubble generators (CCGs): Experiments on a benchmark CAV2003 hydrofoil," *Int. J. Multiphase Flow* **125**, 103186 (2020).
- ¹⁸⁴B. Che and D. Wu, "Study on vortex generators for control of attached cavitation," in *Fluids Engineering Division Summer Meeting* (2017).
- ¹⁸⁵P. K. Kundu, I. M. Cohen, and D. R. Dowling, "Chapter 11—Instability," in *Fluid Mechanics* (Academic Press, Boston, 2016).
- ¹⁸⁶B. Che, N. Chu, L. Cao, S. J. Schmidt, D. Likhachev, and D. Wu, "Control effect of micro vortex generators on attached cavitation instability," *Phys. Fluids* **31**, 064102 (2019).
- ¹⁸⁷N. Qiu, W. Zhou, B. Che, D. Wu, L. Wang, and H. Zhu, "Effects of microvortex generators on cavitation erosion by changing periodic shedding into new structures," *Phys. Fluids* **32**, 104108 (2020).
- ¹⁸⁸H.-B. Huang, Y. Long, and B. Ji, "Experimental investigation of vortex generator influences on propeller cavitation and hull pressure fluctuations," *J. Hydrodyn.* **32**, 82 (2020).
- ¹⁸⁹L. Li, B. Zhou, H. Huang, and H. Sun, "Vortex generator design and numerical investigation for wake non-uniformity and cavitation fluctuation pressure reduction," *Ocean Eng.* **229**, 108965 (2021).
- ¹⁹⁰O. Teplov and V. Lomakin, "Improving the performance of a centrifugal vane pump by installing vortex generators on the suction surfaces of blades," *IOP Conf. Ser.: Mater. Sci. Eng.* **779**, 012012 (2020).
- ¹⁹¹J. Chen, C. Hu, M. Zhang, B. Huang, and H. Zhang, "The influence of micro vortex generator on inception cavitation," *Phys. Fluids* **33**, 103312 (2021).